

# Understanding transport simulations of heavy-ion collisions at 100 and 400 AMeV – A comparison of heavy ion transport codes under controlled conditions

Jun Xu,<sup>1,\*</sup> Lie-Wen Chen,<sup>2,†</sup> ManYee Betty Tsang,<sup>3,‡</sup> Hermann Wolter,<sup>4,§</sup> Ying-Xun Zhang,<sup>5,¶</sup> Joerg Aichelin,<sup>6</sup> Maria Colonna,<sup>7</sup> Dan Cozma,<sup>8</sup> Pawel Danielewicz,<sup>3</sup> Zhao-Qing Feng,<sup>9</sup> Arnaud Le Fèvre,<sup>10</sup> Theodoros Gaitanos,<sup>11</sup> Christoph Hartnack,<sup>6</sup> Kyungil Kim,<sup>12</sup> Youngman Kim,<sup>12</sup> Che-Ming Ko,<sup>13</sup> Bao-An Li,<sup>14</sup> Qing-Feng Li,<sup>15</sup> Zhu-Xia Li,<sup>5</sup> Paolo Napolitani,<sup>16</sup> Akira Ono,<sup>17</sup> Massimo Papa,<sup>18</sup> Taesoo Song,<sup>19</sup> Jun Su,<sup>20</sup> Jun-Long Tian,<sup>21</sup> Ning Wang,<sup>22</sup> Yong-Jia Wang,<sup>15</sup> Janus Weil,<sup>19</sup> Wen-Jie Xie,<sup>23</sup> Feng-Shou Zhang,<sup>24</sup> and Guo-Qiang Zhang<sup>1</sup>

<sup>1</sup>Shanghai Institute of Applied Physics, Chinese Academy of Sciences, Shanghai 201800, China

<sup>2</sup>Department of Physics and Astronomy and Shanghai Key Laboratory for Particle Physics and Cosmology, Shanghai Jiao Tong University, Shanghai 200240, China

<sup>3</sup>National Superconducting Cyclotron Laboratory and Department of Physics and Astronomy, Michigan State University, East Lansing, Michigan 48824, USA

<sup>4</sup>Fakultät für Physik, Universität München, D-85748 Garching, Germany

<sup>5</sup>China Institute of Atomic Energy, Beijing 102413, P.R. China

<sup>6</sup>SUBATECH, UMR 6457, Ecole des Mines de Nantes - IN2P3/CNRS - Université de Nantes, France

<sup>7</sup>INFN-LNS, Laboratori Nazionali del Sud, 95123 Catania, Italy

<sup>8</sup>IFIN-HH, Reactorului 30, 077125 Măgurele-Bucharest, Romania

<sup>9</sup>Institute of Modern Physics, Chinese Academy of Sciences, Lanzhou 730000, People's Republic of China

<sup>10</sup>GSI Helmholtzzentrum für Schwerionenforschung, Darmstadt, Germany

<sup>11</sup>Department of Theoretical Physics, Aristotle University of Thessaloniki, GR-54124 Thessaloniki, Greece

<sup>12</sup>Rare Isotope Science Project, Institute for Basic Science, Daejeon 305-811, Korea

<sup>13</sup>Cyclotron Institute and Department of Physics and Astronomy, Texas A&M University, College Station, Texas 77843, USA

<sup>14</sup>Department of Physics and Astronomy, Texas A&M University-Commerce, Commerce, TX 75429-3011, USA

<sup>15</sup>School of Science, Huzhou University, Huzhou 313000, China

<sup>16</sup>IPN, CNRS/IN2P3, Université Paris-Sud 11, 91406 Orsay cedex, France

<sup>17</sup>Department of Physics, Tohoku University, Sendai 980-8578, Japan

<sup>18</sup>INFN - Sezione di Catania, 95123 Catania, Italy

<sup>19</sup>Frankfurt Institut for Advanced Studies and Institute for Theoretical Physics, Johann Wolfgang Goethe Universität, Frankfurt am Main, Germany

<sup>20</sup>Sino-French Institute of Nuclear Engineering & Technology, Sun Yat-sen University, Zhuhai 519082, China

<sup>21</sup>College of Physics and Electrical Engineering, Anyang Normal University, Anyang, Henan 455000, China

<sup>22</sup>Department of Physics and Technology, Guangxi Normal University, Guilin 541004, China

<sup>23</sup>Department of Physics, Yuncheng University, Yuncheng 044000, China

<sup>24</sup>Key Laboratory of Beam Technology and Material Modification of Ministry of Education, College of Nuclear Science and Technology, Beijing Normal University, Beijing 100875, China

Transport simulations are very valuable for extracting physics information from heavy-ion collision experiments. With the emergence of many different transport codes in recent years, it becomes important to estimate their robustness in extracting physics information from experiments. We report on the results of a transport code comparison project. 18 commonly used transport codes were included in this comparison: 9 Boltzmann-Uehling-Uhlenbeck-type codes and 9 Quantum-Molecular-Dynamics-type codes. These codes have been required to simulate Au+Au collisions using the same physics input for mean fields and for in-medium nucleon-nucleon cross sections, as well as the same initialization set-up, the impact parameter, and other calculational parameters at 100 and 400 AMeV incident energy. Among the codes we compare one-body observables such as rapidity and transverse flow distributions. We also monitor non-observables such as the initialization of the internal states of colliding nuclei and their stability, the collision rates and the Pauli blocking. We find that not completely identical initializations constitute partly for different evolutions. Different strategies to determine the collision probabilities, and to enforce the Pauli blocking, also produce considerably different results. There is a substantial spread in the predictions for the observables, which is much smaller at the higher incident energy. We quantify the uncertainties in the collective flow resulting from the simulation alone as about 30% at 100 AMeV and 13% at 400 AMeV, respectively. We propose further steps within the code comparison project to test the different aspects of transport simulations in a box calculation of infinite nuclear matter. This should, in particular, improve the robustness of transport model predictions at lower incident energies where abundant amounts of data are available.

PACS numbers: 24.10.Lx, 25.70.-z, 21.30.Fe

## I. INTRODUCTION

Understanding the behavior of nuclear systems in a wide range of densities, temperatures, and proton-neutron asymmetries, characterized by the equation of state (EoS) of nuclear matter, is one of the major goals in nuclear physics research. As the main characteristic of bulk nuclear matter, the EoS is also an important input to the study of astrophysical objects or processes like neutron stars or core collapse supernovae. In the laboratory, the EoS has been studied with heavy-ion collisions (HIC), which can create a wide range of density and energy conditions depending on the incident energy of the collision, the size of the colliding system, and impact parameters. The EoS is not observed directly, but has to be inferred from the properties of reaction products. At lower energies, heavy-ion collisions are interpreted with considerable success by statistical models. Since heavy-ion collisions are dynamical processes, the preferred method relies on non-equilibrium theories, which model the reaction and have as inputs the EoS, effective nucleon-nucleon (NN) cross sections, effective nucleon masses, and other physics quantities used in the models. For the energies under consideration here, i.e., from the Fermi energy regime to relativistic energies, transport theories are an important tool to obtain valuable information from heavy-ion collisions.

Transport theories have been used for many years, starting from the early works of Refs. [1–3], to interpret heavy-ion collisions. Their use has achieved remarkable success. For example, the EoS has been constrained rather well for symmetric nuclear matter [4–7] with transport models. On the other hand, the isovector sector of the EoS, i.e., the nuclear symmetry energy or Asy-EoS, which is of great importance for the astrophysical applications, is still less known. Even though constraints for the symmetry energy are becoming increasingly stringent [8–14], there are still large uncertainties particularly above saturation densities. For the investigation of the symmetry energy which contributes only a fraction of the total energy, but the influence of which increases with the asymmetry of nuclear systems, an increased precision of the prediction of transport theories is required (for a recent review, see Ref. [15]).

Recently, different transport models have given different predictions for physical observables with seemingly similar nuclear input. Considering the different approaches to transport theory, it is important to disentangle the causes that lead to different predictions via, e.g., the transport code comparison project. One of the goals of the code comparison project is to establish a theoretical systematic error that quantifies the model dependence of transport predictions. Our eventual goal is to minimize this error even if it may not be possible to get an exact convergence of the results from different transport codes.

Possible reasons for the model dependence are inherent in the complexity of transport calculations. Basically two families of transport approaches are used in the study of heavy-ion collisions. One is the Boltzmann-Vlasov type, which is formulated for the evolution of the one-body phase-space density under the influence of a mean field. The other is the molecular dynamics type, which is formulated in terms of nucleon coordinates and momenta under the action of a many-body Hamiltonian. Both are supplemented with a two-body collision term. There are many variants of these two basic approaches. We will refer to the first type of theories collectively as Boltzmann-Uehling-Uhlenbeck (BUU) theories, and to the second as Quantum Molecular Dynamics (QMD) theories, according to their most common representatives. The equations of these theories are generally solved by numerical simulations due to their complexity. Different strategies are used in BUU- and QMD-type models, but also in individual codes within each family. These differences are not always evident in publications when results are presented. Simulations to interpret experimental data often employ different physical inputs and slightly different conditions, such that the results may not be directly compared, and the model uncertainties cannot be separated from the variations of the physical input. To provide a better understanding of these differences, all calculations shown in the present work use exactly the same physical input and, as closely as possible, the same initial conditions.

It has long been recognized that a comparison between different transport models is very much needed. In 2004 the community met at the European Center for Theoretical Studies for Nuclear Physics and Related Fields (ECT\*) in Trento, Italy, to compare mainly the particle production and also yields, rapidity distributions, and transverse spectra from various transport codes in the 1 AGeV regime. Results from that comparison were published in Ref. [16]. Following this first step, an attempt was made to compare bulk observables, namely anisotropies of momentum distributions (flow) and collision rates, at lower energies (100 and 400 AMeV) in a workshop in Trento in 2009. While anisotropies of momentum distributions are widely used in the analyses of HIC, it became evident that their prediction is much less robust than that of the particle production at higher energies. The Trento workshop was followed by the

---

\*Electronic address: xujun@sinap.ac.cn

†Electronic address: lwchen@sjtu.edu.cn

‡Electronic address: tsang@nscl.msu.edu

§Electronic address: hermann.wolter@physik.uni-muenchen.de

¶Electronic address: zhyx@ciae.ac.cn

International Workshop on Simulations of Low- and Intermediate-Energy Heavy-Ion Collisions in 2014, in Shanghai, China [17]. Before, during, and after the meeting, we have compared the calculated results based on 18 transport codes listed in Table I [18]. This list includes the transport codes most widely used by the intermediate-energy heavy-ion community today.

The comparison project, including homework results as well as details of the different codes, will be published by Springer in a special Volume. This article intends to present in a timely manner the relevant results obtained in the first phase of the comparison project, before the book becomes available. Response to this article will be used to improve the contents of the book. Furthermore, we hope that this project will lead to a useful milestone making it possible to better clarify different strategies adopted in the formulation of the transport models.

This article is organized as follows: Brief descriptions of the two families of the most widely used transport models, BUU and QMD, will be given in Sec. II. Section III gives details of the set-up of the calculations, called here the homework of the code comparison, since we asked each participant to provide results of calculations with specified requirements. In Sec. IV the initialization of the collisions will be discussed together with the stability of the initial set-up. This is realized by performing a calculation with a large impact parameter,  $b = 20$  fm, such that an actual nucleus-nucleus collision rarely occurs. In Sec. V we compare the results for a more realistic heavy-ion collision at an intermediate impact parameter,  $b = 7$  fm, to study different observables and collision rates. Here we compare collisions at two energies, 100 and 400 AMeV. At different energies the influence of the mean field and collisions will be different. In fact, it will be seen, that collisions at 100 AMeV represent a particularly critical regime, where there is a strong competition between the mean field and the collisions, and where, therefore, the difference in the codes is magnified. This appears less critical at the higher energy. In Sec. VI a critical discussion of the aims and implications of the present code comparison is presented. Finally in Sec. VII we summarize the results and achievements of this investigation. We also discuss further steps to reach the goal of a better convergence and understanding of different transport models, for which we plan a follow-up calculation for an infinite system of nuclear matter, set up as a calculation in a box with periodic boundary conditions.

In this paper we show some highlight results of the code comparison project, while technical details of all the codes used in the comparison will appear in the book mentioned above. The relevant ingredients of the codes used in the present code comparison project are summarized in Tables II and III containing the information for initialization, nucleon-nucleon scatterings and Pauli Blocking, where appropriate. There are considerable differences in calculating occupation probabilities and treating the Pauli blocking. We stress that the treatment given in these tables is not necessarily the mode in which they are used in applications to data of heavy-ion collisions, which will be given in the book. Until the special volume on the "Transport Code Comparison Project" is published, detailed descriptions of all the codes can be found in the references provided in the tables.

TABLE I: The names, authors and correspondents, and representative references of 9 BUU-type and 9 QMD-type models participating in the transport code comparison project. The intended beam-energy range for each code is given in GeV.

BUU-type	code correspondents	energy range	reference	QMD-type	code correspondents	energy range	reference
BLOB	P.Napolitani,M.Colonna	0.01 ~ 0.5	[19]	AMD	A.Ono	0.01 ~ 0.3	[27]
GIBUU-RMF	J.Weil	0.05 ~ 40	[20]	IQMD-BNU	J.Su,F.S.Zhang	0.05 ~ 2	[28]
GIBUU-Skyrme	J.Weil	0.05 ~ 40	[20]	IQMD	C.Hartnack,J.Aichelin	0.05 ~ 2	[29, 30]
IBL	W.J.Xie,F.S.Zhang	0.05 ~ 2	[21]	CoMD	M.Papa	0.01 ~ 0.3	[31]
IBUU	J.Xu,L.W.Chen,B.A.Li	0.05 ~ 2	[11, 22]	ImQMD-CIAE	Y.X.Zhang,Z.X.Li	0.02 ~ 0.4	[32]
pBUU	P.Danielewicz	0.01 ~ 12	[23]	IQMD-IMP	Z.Q.Feng	0.01 ~ 10	[33]
RBUU	K. Kim,Y.Kim,T.Gaitanos	0.05 ~ 2	[24]	IQMD-SINAP	G.Q.Zhang	0.05 ~ 2	[34]
RVUU	T.Song,G.Q.Li,C.M.Ko	0.05 ~ 2	[25]	TuQMD	D.Coza	0.1 ~ 2	[35]
SMF	M.Colonna,P.Napolitani	0.01 ~ 0.5	[26]	UrQMD	Y.J.Wang,Q.F.Li	0.05 ~ 200	[36, 37]

TABLE II: Initialization and nucleon-nucleon scattering treatment used in various codes in homework calculations.

Code name	Shape of particles	$(\Delta x)^2$ [fm <sup>2</sup> ] <sup>a</sup>	$\delta < r^2 >^{1/2}$ (fm) <sup>b</sup>	$\delta < r^4 >^{1/4}$ (fm) <sup>c</sup>	Attempted collisions	1st collisions within same nucleus
AMD	Gaussian	1.56	-0.01	0.01	$p = \alpha e^{-\nu R_{ij}^2} v_{ij} \Delta t$	yes
IQMD-BNU	Gaussian	1.97	0.32	0.39	Bertsch approach <sup>d</sup>	no
IQMD	Gaussian	2.16	0.64	0.85	Bertsch approach	yes
CoMD	Gaussian	1.32	-0.11	-0.04	$p = 1 - e^{\Delta t/\tau}$	yes
ImQMD-CIAE	Gaussian	2.02	0.39	0.47	Bertsch approach	yes
IQMD-IMP	Gaussian	1.92	0.61	0.80	Bertsch approach	yes
IQMD-SINAP	Gaussian	2.16	0.03	0.12	Bertsch approach	yes
TuQMD	Gaussian	2.16	-0.17	-0.17	Bertsch approach	yes
UrQMD	Gaussian	2	0.12	0.18	collision time table <sup>e</sup>	yes
	Shape of test particle	$(\Delta x)^2$ [fm <sup>2</sup> ] or $l$ [fm] <sup>f</sup>				
BLOB	triangle	2	0.10	0.07	$p = \sigma^{med} \frac{(\rho_i + \rho_j)}{2} v_{ij} \Delta t$	yes
GIBUU-RMF	Gaussian	1	-0.18	-0.26	Bertsch approach	yes
GIBUU-Skyrme	Gaussian	1	-0.03	-0.03	Bertsch approach	yes
IBL	Gaussian	2	-0.32	-0.42	Bertsch approach	no
IBUU	triangle	1	0.01	0.04	Bertsch approach	yes
pBUU	point	0 <sup>g</sup>	0.01	-0.02	cell <sup>h</sup>	yes
RBUU	invar.Gauss	1.4	-0.12	-0.19	Bertsch approach	yes
RVUU	point	0	0.01	0.03	Bertsch approach	yes
SMF	triangle	2	-0.13	-0.18	$p = \sigma^{med} \frac{(\rho_i + \rho_j)}{2} v_{ij} \Delta t$	yes

<sup>a</sup> $\Delta x$  is the width of the Gaussian wavepacket as in Eq. (6).

<sup>b</sup> $\delta < r^2 >^{1/2} = \langle r^2 >^{1/2} - \langle r^2 >_{WS}^{1/2}$  with  $\langle r^2 >_{WS}^{1/2}$  from the required Woods-Saxon distribution.

<sup>c</sup> $\delta < r^4 >^{1/4} = \langle r^4 >^{1/4} - \langle r^4 >_{WS}^{1/4}$  with  $\langle r^4 >_{WS}^{1/4}$  from the required Woods-Saxon distribution.

<sup>d</sup>"Bertsch approach" means:  $b < \sqrt{\sigma^{med}/\pi}$  and  $v_{ij} \gamma \Delta t / 2 > |r_{ij} \cdot \vec{p}/p|$  as described in the Appendix B of Ref. [38].

<sup>e</sup>Details about the collision criterion in UrQMD can be found in Ref. [37]

<sup>f</sup> $l$  is the lattice spacing for test particle with triangular shape. See its definition in Ref. [39].

<sup>g</sup>The node separation for the calculation of average quantities is typically 0.92 fm, but can decrease with increasing energy. See Ref. [23] for details.

<sup>h</sup>See Ref. [40] for details.

TABLE III: Pauli-blocking treatment used in various codes in homework calculations.

Code name	Occupation probability $f_i$	Blocking probability <sup>a</sup>	Additional constraints
AMD	antisymmetrized wavepackets <sup>b</sup>	physical wavepacket <sup>b</sup>	no
IQMD-BNU	$f_i$ in $h^3$	$1 - (1 - f_i)(1 - f_j)$	yes <sup>c</sup>
IQMD	$f_i$ in $h^3$	$1 - (1 - f_i)(1 - f_j)$	yes <sup>d</sup>
CoMD	$f_i$ in $h^3$	$f'_i, f'_j < f_{\max} = 1.05 - 1.1$	yes <sup>e</sup>
ImQMD-CIAE	$f_i$ in $h^3$	$1 - (1 - f_i)(1 - f_j)$	no
IQMD-IMP	$f_i$ in phase-space cell with $dx = 3.367$ fm, $dp = 89.3$ MeV/c	$1 - (1 - f_i)(1 - f_j)$	no
IQMD-SINAP	$f_i = \sum_k e^{-(\vec{r}_k - \vec{r}_i)^2 / [2(\Delta x)^2]} e^{-(\vec{p}_k - \vec{p}_i)^2 \cdot 2(\Delta x)^2 / \hbar^2}$	$1 - (1 - f_i)(1 - f_j)$	no
TuQMD	$f_i$ in spherical phase-space cell with $dx = 3.0$ fm, $dp = 240$ MeV/c <sup>f</sup>	$1 - (1 - f_i)(1 - f_j)$	yes <sup>g</sup>
UrQMD	$f_i = \sum_k e^{-(\vec{r}_k - \vec{r}_i)^2 / [2(\Delta x)^2]} e^{-(\vec{p}_k - \vec{p}_i)^2 \cdot 2(\Delta x)^2 / \hbar^2}$	$1 - (1 - f_i)(1 - f_j)$	yes <sup>h</sup>
BLOB	$f_i$ in sphere with radius 3.5 fm with Gaussian weight in momentum space <sup>i</sup>	$1 - (1 - f_i)(1 - f_j)$	yes <sup>j</sup>
GIBUU-RMF	$f_i$ in phase-space cell with $dx = 1.4$ fm, $dp = 68$ MeV/c	$1 - (1 - f_i)(1 - f_j)$	no
GIBUU-Skyrme	$f_i$ in phase-space cell with $dx = 1.4$ fm, $dp = 68$ MeV/c	$1 - (1 - f_i)(1 - f_j)$	no
IBL	$f_i$ in $h^3$	$1 - (1 - f_i)(1 - f_j)$	yes <sup>k</sup>
IBUU	$f_i$ in phase-space cell with $dx = 2.73$ fm, $dp = 187$ MeV/c	$1 - (1 - f_i)(1 - f_j)$	no
pBUU	$f_i$ in same and neighboring spatial cell <sup>l</sup>	$1 - (1 - f_i)(1 - f_j)$	no
RBUU	$f_i$ in phase-space cell with $dx = 1.4$ fm, $dp = 64$ MeV/c	$1 - (1 - f_i)(1 - f_j)$	no
RVUU	$f_i$ in phase-space cell with $dx = 1.14$ fm, $dp = 331$ MeV/c <sup>m</sup>	$1 - (1 - f_i)(1 - f_j)$	no
SMF	$f_i$ in sphere with radius 2.53 fm with Gaussian weight in momentum space <sup>n</sup>	$1 - (1 - f_i)(1 - f_j)$	no

<sup>a</sup>Occupation probability  $f_i$  is replaced by  $\min[f_i, 1]$  if  $f_i$  is larger than 1.

<sup>b</sup>See Ref. [27] for details.

<sup>c</sup>Phase-space constraint, see Ref. [28] for details.

<sup>d</sup>Isospin average, see Ref. [29] for details.

<sup>e</sup>Phase-space constraint, see Ref. [41] for details.

<sup>f</sup>In TuQMD the Pauli Blocking is implemented by computing the wave function overlap using the method described in Ref. [30].

<sup>g</sup>Surface modification, see Ref. [42] for details.

<sup>h</sup>Phase-space constraint:  $\frac{4\pi}{3} r_{ik}^3 \frac{4\pi}{3} p_{ik}^3 \geq \left(\frac{\hbar}{2}\right)^3 / 4$ .

<sup>i</sup>Width of the Gaussian from definition of test-particle agglomerates, see Ref. [19] for details.

<sup>j</sup>Wavepacket modulation (shape, widths) to ensure strict Pauli blocking.

<sup>k</sup>Fermi constraint, see Ref. [21] for details.

<sup>l</sup>See Ref. [23] for details.

<sup>m</sup>Obtained using  $dx = [3/(4\pi\rho_0)]^{1/3}$  and  $dp = [6\pi^2\rho_0/(2s+1)]^{1/3}$ , see Ref. [25] for details.

<sup>n</sup>The width of the Gaussian is 29 MeV/c.

## II. BRIEF DESCRIPTION OF TRANSPORT THEORIES

Transport theories are very useful for extracting physical information on nuclear matter from heavy-ion collisions. In this section we briefly characterize the two main approaches for transport simulations. This is thus not intended as a comprehensive theoretical discussion of the derivation and validity of transport theories, but rather as a "technical"

guide of the main characteristics, the methods of implementation, and the ingredients and methods to perform transport simulations in order to facilitate the discussion of the code comparisons in this paper.

Transport theories describe the evolution of the one-body phase-space distribution in a heavy-ion collision under the action of a mean field, two-body collisions, and their Pauli blocking. To which extent higher-order correlations are taken into account will be discussed below. There are essentially two approaches to solve the problem: those, which evolve directly from the phase-space density, generally called here Boltzmann-Uehling-Uhlenbeck (BUU) approaches [38], and those, which formulate the transport in terms of nucleon coordinates and momenta, generally called here Quantum Molecular Dynamics (QMD) approaches [29, 30]. There are both relativistic and non-relativistic formulations of each approach. Table I lists the names, the authors and correspondents, the intended energy range, and the main reference of each code, that participates in this comparison.

### A. The Boltzmann-Uehling-Uhlenbeck approach

The BUU theory can be derived from the Born-Bogoliubov-Green-Kirkwood-Yvon (BBGKY) hierarchy or from some perspective more effectively, using the real time Green function Martin-Schwinger formalism to arrive at the Kadanoff-Baym equations [43–45]. With the quasi-particle approximation (on-shell particles), an approximation for the (complex) self energy, and a semi-classical approximation, one arrives at the Boltzmann-Uehling-Uhlenbeck (BUU) equation for the phase-space density. The equation describes the time evolution of the one-body phase-space density  $f(\vec{r}, \vec{p}; t)$

$$\left( \frac{\partial}{\partial t} + \frac{\vec{p}}{m} \cdot \nabla_r - \nabla_r U \cdot \nabla_p \right) f(\vec{r}, \vec{p}; t) = I_{coll}[f; \sigma_{12}] \quad (1)$$

under the influence of the mean field  $U[f]$  (usually formulated as a density functional depending on the baryon density as well as the isospin and possibly spin and assumed here to be momentum independent) and a two-body collision term

$$I_{coll} = \frac{1}{(2\pi)^6} \int dp_2 dp_3 d\Omega |v - v_2| \frac{d\sigma_{12}^{med}}{d\Omega} (2\pi)^3 \delta(p + p_2 - p_3 - p_4) \\ \times [f_3 f_4 (1 - f)(1 - f_2) - f f_2 (1 - f_3)(1 - f_4)] \quad (2)$$

where  $\sigma^{med}$  is the in-medium nucleon-nucleon cross section and assumed here to be elastic. The left-hand side of Eq. (1) is the Vlasov equation, which can be derived as a semi-classical approximation to the time-dependent Hartree-Fock (TDHF) equation. The UU (Uehling-Uhlenbeck) abbreviation in the BUU equation stands for the introduction of the Pauli blocking factors in the gain and loss terms of the collision. Other names for the same equation are Vlasov-Uehling-Uhlenbeck (VUU), Boltzmann-Nordheim-Vlasov (BNV), or Landau-Vlasov (LV). The physical ingredients in the BUU equation are the mean field  $U$  and the in-medium cross section  $\sigma^{med}$ . The derivation sketched above can give a consistent approximation for both quantities, e.g., from the closed-time path Green function method as in Ref. [45]. However, in many applications, and also in this code comparison, these are specified independently. This allows us to test which observables are sensitive to which ingredients.

The BUU equation is a non-linear integral-differential equation which cannot be solved analytically or in a direct numerical way. Rather the common method is to simulate the solution by using the test-particle (TP) technique, which was introduced to nuclear physics in the beginning of 80s by Wong [46] for the solution of the TDHF equation. Here the (continuous) distribution function is resolved in terms of a (large) number of discrete TPs as

$$f(\vec{r}, \vec{p}; t) = \frac{1}{N_{TP}} \sum_{i=1}^{N_{TP} A} g(\vec{r} - \vec{r}_i(t)) \tilde{g}(\vec{p} - \vec{p}_i(t)) \quad (3)$$

where  $A$  is the number of nucleons,  $N_{TP}$  is the test particle number per nucleon (100 in this work),  $\vec{r}_i$  and  $\vec{p}_i$  are the coordinates and momenta of the test particles, and  $g$  and  $\tilde{g}$  are the coordinate and momentum shapes. The coordinate shape is often taken as point particles ( $\delta$  functions), but to reduce the number of test particles and make the distribution smoother, it may be taken as Gaussians or triangular shapes in some codes (see Table II). A finite shape in momentum space is not commonly used, but becomes relevant for momentum-dependent interactions or in the calculation of momentum dependent quantities. It can be shown, that approximatively under the influence of the mean field, the test particle coordinates and momenta obey the Hamiltonian equations of motion

$$d\vec{r}_i/dt = \nabla_{\vec{p}_i} H; \quad d\vec{p}_i/dt = -\nabla_{\vec{r}_i} H. \quad (4)$$

One usually has to average the density over a cell (typically of size  $1 \text{ fm}^3$ ), which is equivalent to a coarse-graining in the solutions of the equations.

The collision term is commonly simulated stochastically, performing TP collisions with cross section  $\sigma' = \sigma^{med}/N_{TP}$ . At each time step the TP configuration is sampled to find TPs which are closer than the geometrical limit  $d = \sqrt{\sigma'/\pi}$  to make a collision. Sometimes additional constraints are introduced, such as not allowing two collisions of the same TP in the same time step, making sure that the two TPs move towards each other, or requiring that the first collision of two TPs are not in the same nucleus, etc (see Table III). For each such "attempted" collision, the Pauli blocking is checked by calculating the phase-space occupation for the final states. Here an average over a final cell has to be taken to obtain reasonably smooth results, also a type of coarse-graining. The Pauli blocking probability is calculated in most cases from  $1 - (1 - f_3)(1 - f_4)$  (see Table III). This still leads to an over-occupation of a final cell. Some codes then disallow the collision (or force the occupation to have the value 1). In principle with Fermi statistics implemented at the beginning of the reaction and the Pauli principle enforced in the collision term, the Fermion nature of the system should be preserved in the evolution. However, it has been shown [47] that the coarse-graining can act as a dissipation which evolves the statistics to a classical Maxwell-Boltzmann distribution.

The above method of solving the collision term, called the full ensemble method, is numerically expensive since it scales like  $(AN_{TP})^2$ . In most calculations the parallel ensemble method is used, where the total number of test particles is divided into  $N_{TP}$  ensembles of  $A$  particles each. Then collisions are allowed to occur only in each ensemble with cross section  $\sigma^{med}$ , while the Pauli blocking and the mean field are calculated by using the test particles from all the ensembles. It has been checked in typical cases that this procedure gave results similar to the full ensemble method.

## B. The Quantum Molecular Dynamics Approach

The QMD approach to transport theory can be discussed from two perspectives. It has a relation to classical molecular dynamics for the nucleons with a Hamiltonian, which is formulated in terms of two- or many-body interactions (but often also in terms of density functionals). The nucleons are specified not as point particles but as particles with finite widths usually of Gaussian shape. On the other hand QMD can be derived from a time-dependent Hartree (TDH) theory with a trial wave function of a product of Gaussian single-particle wave functions  $\phi_i(\vec{r}; t)$  with positions  $\vec{R}_i(t)$  and momenta  $\vec{P}_i(t)$  as variational parameters [30]

$$\Psi(\vec{r}_1, \dots, \vec{r}_N; t) = \prod \phi_i(\vec{r}_i; t), \quad (5)$$

$$\phi_i(\vec{r}_i; t) = \frac{1}{(2\pi)^{3/4}(\Delta x)^{3/2}} \exp \left[ -\frac{(\vec{r}_i - \vec{R}_i(t))^2}{(2\Delta x)^2} + i\vec{r}_i \cdot \vec{P}_i(t) \right]. \quad (6)$$

The variation of the wave function, Eq. (5), leads to equations of motion for the nucleons which are very similar to BUU, i.e., the same Eqs. (4) are valid for the centroids of Gaussian wave function in coordinate and momentum space  $\vec{R}_i(t)$  and  $\vec{P}_i(t)$ , with  $\vec{R}_i = \langle \vec{r}_i \rangle$  and  $\vec{P}_i = \langle \vec{p}_i \rangle$ . Thus large differences in the propagation are not expected for one-body observables. For AMD (antisymmetrized molecular dynamics) [27] or FMD (fermionic molecular dynamics) [48] approach, the antisymmetrization of the wavepackets is taken into account, i.e., as derived from TDHF with a Slater determinant of Gaussians as a trial wave function. The equations of motion become more complicated, involving a norm matrix, since wavepacket overlap changes when they move (for more details see Ref. [27]). A variant of this approach is CoMD (constrained molecular dynamics), which does not explicitly implement antisymmetrization, but takes the effects into account in an effective interaction [31]. The single particle Gaussians in QMD usually have a fixed width, while the change of the wavepacket shape is taken into account in a version of AMD as the wavepacket splitting [49].

In QMD approaches the two-body collisions are also introduced, and are simulated in much the same way as in the full ensemble technique of BUU, see the preceding subsection that applies to QMD for the nucleon coordinates and the full in-medium cross section  $\sigma^{med}$ . In both cases nucleons (not test particles) collide with the NN in-medium cross section. Thus a collision will affect the distribution function considerably more than a TP collision in BUU. The treatment of collisions in QMD approaches is intrinsically stochastic. In contrast to BUU, two-nucleon collisions induce event-by-event fluctuations. A large number of runs are performed (with different initial states), which are considered as "events" and which are averaged to obtain the mean and the variation of the final result.

The above discussion also touches the question in which way any higher-order correlations not captured by the one-body distribution function are included in QMD approaches. Due to the form of the trial wave function, QMD can probably describe classical N-body correlations better than the BUU approach. On the other hand, the relation of QMD to TDH shows that no quantum correlations can be present beyond the mean-field level. These questions demand more detailed discussions and are beyond the scope of this section.

### C. Fluctuations

Even though fluctuations are probably not important in the simulations of the present code comparison, which looks only at global one-body observables, they become critically important in cluster formation. Fluctuations are also relevant to the question of the initialization of a heavy-ion collision, which is treated in more detail in Sec. IV. Here we discuss in general how fluctuations arise in the BUU and QMD approaches.

In BUU the TP simulation yields an exact solution of the BUU equation in the limit of an infinite number of TPs. Thus BUU is a deterministic equation, and in the above limit one obtains a unique solution with no fluctuations. Fluctuations appear in practice, because of the finite number of TPs and the stochastic simulation of the collision term. These fluctuations are unphysical (but early on they were used to gauge the most unstable mode of the system [50]). However, from a physical point of view the BUU transport theory should be extended to include fluctuations since dissipation (collision term) should always be accompanied by fluctuations [47]. Additional sources of fluctuation arise from initial correlations and from the truncation of higher-order correlations. The inclusion of fluctuations leads to the Boltzmann-Langevin equation with the addition of a fluctuation term on the right-hand side of Eq. (1) [47]. Recently methods were devised to introduce fluctuations, from the early BOB method (Brownian one-body fluctuation [51]), to the SMF (stochastic mean field) formulation with density fluctuations [26], and to the most recent BLOB (Boltzmann-Langevin one body) approach [19]. The latter approach implements fluctuations by a method modified from the original proposal of Ref. [52], which moves with one TP collision a swarm of  $N_{TP}$  test particles, corresponding to a nucleon-nucleon collision. In this sense it is closer to QMD with respect to the collision statistics.

Due to its relation to molecular dynamics, QMD-type theories include classical N-body correlations, and thus are expected to show more fluctuations than BUU-type theories. The width parameter of the Gaussians  $\Delta x$ , usually taken in the range about  $(\Delta x)^2 \sim 1 - 2 \text{ fm}^2$ , can be considered as a parameter to give a reasonable amount of fluctuations and a good reproduction of the surface properties of a nucleus. Note that QMD can be regarded as a similar method to the parallel ensemble technique for BUU but without averaging over ensembles (or events) for the mean field and the Pauli blocking. As discussed above fluctuations will affect fragmentation in heavy-ion collisions. Indeed, a dedicated comparison of AMD and SMF actually showed a considerable difference in cluster yields [53] with different fluctuation treatments in coordinate as well as in momentum space.

### III. HOMEWORK DESCRIPTION

The goal of this paper is a comparison of results between codes but not of code results to experiment. Here we compare the results from different transport models under strictly controlled conditions. Controlled conditions imply not only the same physical input, i.e., the same nuclear EoS and in-medium cross sections, but also initial conditions of the reaction which are set up as close as possible to each other, and are subject to the same requirements on the accuracy of the simulation and the statistical significance. As in the Trento 2009 workshop, Au+Au reactions at 100 and 400 AMeV have been chosen as representative cases. From the history of the code comparison and also for ease of reference, calculations for the two different energies, 100 AMeV and 400 AMeV, are referred as B- and D-mode respectively in this article.

In the homework, we specify the physics input precisely. The nuclear EoS was specified as follows. In the case of non-relativistic transport codes, the code practitioners were told to use the simple Skyrme-type single-nucleon potential

$$U_{n/p} = \alpha \left( \frac{\rho}{\rho_0} \right) + \beta \left( \frac{\rho}{\rho_0} \right)^\gamma \pm 2S_{pot} \left( \frac{\rho}{\rho_0} \right) \delta, \quad (7)$$

where the parameters for the isoscalar potential are  $\alpha = -209.2 \text{ MeV}$ ,  $\beta = 156.4 \text{ MeV}$ , and  $\gamma = 1.35$ , and the strength of the symmetry potential at saturation density is  $S_{pot} = 18 \text{ MeV}$ . In the above  $\delta = (\rho_n - \rho_p)/\rho$  is the isospin asymmetry, and sign + is for neutrons and - for protons. In the case of relativistic transport codes, the code practitioners were told to use the  $NL\rho$  parameterization in the  $\sigma\omega\rho$  relativistic mean-field model, with the values of the parameters from Set I in Ref. [54]. Both the non-relativistic and relativistic nuclear EoS yields the same saturation properties of nuclear matter, i.e., the saturation density of  $\rho_0 = 0.16 \text{ fm}^{-3}$ , the nuclear binding energy  $E_0 = -16 \text{ MeV}$ , the incompressibility  $K_0 = 240 \text{ MeV}$ , and the symmetry energy  $S(\rho_0) = 30.3 \text{ MeV}$ . A Landau model with similar saturation characteristics is used for pBUU [23].

For a better representation of nuclear surface in nuclei, many codes use a surface term, which is proportional to the density gradient or is represented by a Yukawa potential. Since this introduces different behavior in the comparison of the codes, which are difficult to ascertain, we asked the code practitioners to turn off this option.



Regarding elementary processes, the code practitioners were told to suppress inelastic processes and to use constant isotropic cross section of 40 mb for elastic nucleon-nucleon scatterings.

The first step in a simulation is the specification of the initialization of the colliding nuclei, which depends on the methods chosen to represent the phase-space distribution, namely on point or extended test particles in BUU or the shape of the nucleon wavepackets in QMD with or without antisymmetrization. As the simplest prescription, the code practitioners were asked to follow an initial density distribution of Woods-Saxon form

$$\rho(r) = \frac{\rho_0}{1 + \exp[(r - R)/a]}, \quad (8)$$

where  $\rho_0 = 0.16 \text{ fm}^{-3}$  is the saturation density,  $R = 1.12A^{1/3} \text{ (fm)}$  is the nuclear radius, with  $A = 197$  for Au nucleus, and  $a = 0.6 \text{ fm}$  is the diffuseness parameter. As discussed later, it is not easy to obtain an exactly identical initialization, thus we asked the code practitioners to map their initial density distributions as closely as possible using the type of test particle or particle distribution in their codes. Once the coordinate space is sampled, the local density approximation is used to sample the momentum of each nucleon, i.e., the momentum of each (test) particle should be chosen randomly in the local Fermi sphere according to the local density, generally isospin-dependently. The initial distance between the centers of the projectile nucleus and the target nucleus should be set to 16 fm in the beam direction.

The representation of the phase space is different in BUU- and QMD-type models, which also affects the statistical significance of the calculations. To make these approximately comparable, we made the following specifications: 100 test particles per nucleon and 10 simulations with different initializations for BUU models; 1000 simulations with different initializations for QMD models. Since it is difficult to generate 1000 stable initial configurations for QMD models, sometimes they have been generated by rotating a few stable initializations randomly in space. The time evolution of the simulations is followed until 140 fm/c at 100 AMeV and 100 fm/c at 400 AMeV. The time step in the evolution is left to the code practitioners, but is recommended to be set as 0.5 fm/c.

Transport calculations basically have two main ingredients, the mean field (related to EoS), and the NN collisions, which have different influence on the reaction dynamics. It is important to understand the influence of these ingredients in the codes. Therefore, in addition to the full calculations that include both the mean field and NN collisions, we also asked for B-Vlasov calculations, using only the mean field and turning off collisions, and for B-Cascade calculations, with only collisions and no mean field. Note that B mode refers to simulations at the incident energy of 100 AMeV.

For the output of the calculations we asked for the full information from the code practitioners, to make it possible to generate the observables in the same way for all codes and also to be able to inspect additional quantities later on. A transport calculation has the advantage that one may look into the collision at any stage of the evolution, something one cannot do in experiments. The code practitioners provided two types of files: (test) particle files which specify the type, position, and momentum of each (test) particle at times 0, 20, 40, 60, 80, 100, 120, and 140 fm/c for each simulation; collision files, which specifies the type, (effective) mass, time, and momentum of the two colliding (test) particles for each attempted collision, and the result of the Pauli blocking (successful or not). From these files we generated several quantities which are discussed in the next two sections.

#### IV. INITIAL CONFIGURATIONS AND STABILITY

Ideally all codes should start with the same initial configurations so that one can disentangle the effects of the initial conditions and the reaction dynamics. Although the initial density distributions of a Woods-Saxon form was detailed in the homework, as described in Sec. III, this procedure for the initialization turned out to be not quite satisfactory, since it does not guarantee that the initial nuclei are really in the ground state corresponding to the nuclear mean field chosen in the homework. To check the stability of the initial configurations, simulations were first performed at a large impact parameter,  $b = 20 \text{ fm}$ , so that the projectile and target were far enough apart that essentially no nucleons or energy should be exchanged. The mean density evolution of an Au nucleus obtained from an average of the projectile and target nuclei was then used to check the stability of the initial configurations.

##### A. Initial Configurations

There are many treatments for the initialization of the nuclei. For instance, nucleons may be treated as point particles, Gaussian-type finite-size particles [29, 30], or triangular-type finite-size particles [19, 26], and in QMD models the width of Gaussian wavepacket depends on the size of the collision system [30, 55]. Generally, BUU-type models use a given density distribution provided by a Woods-Saxon parameterization, the Skyrme-Hartree-Fock calculation [56], or the Thomas-Fermi approximation [23, 39]. For QMD-type models, the initial configurations of

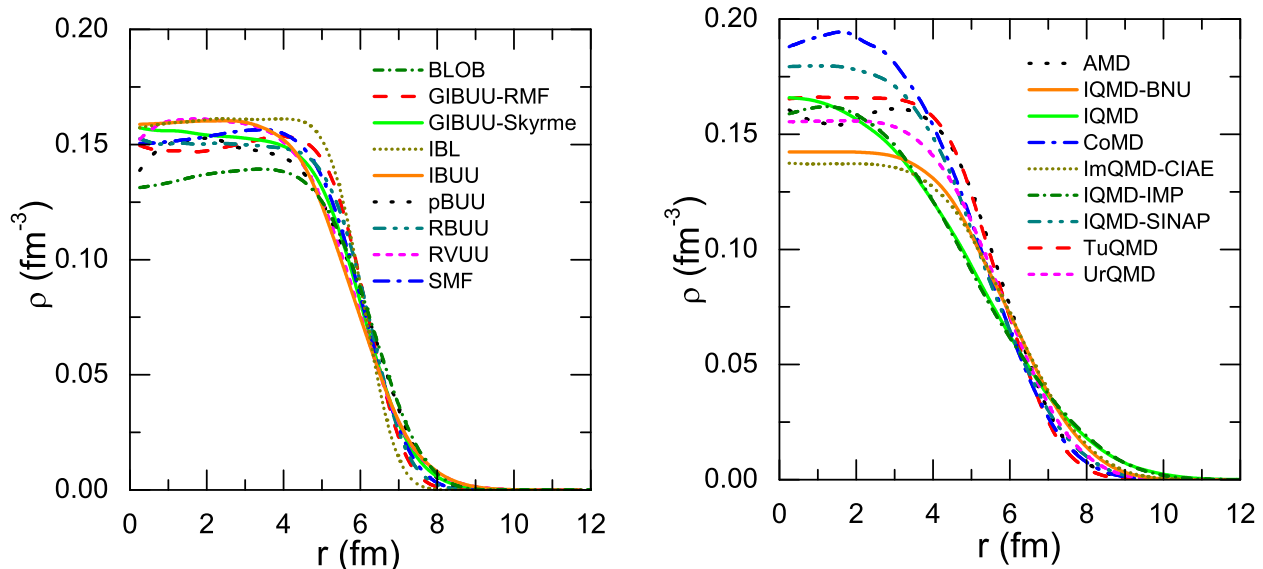


FIG. 1: (Color online) Initial density profiles for BUU-type (left panel) and QMD-type (right panel) models.

nuclei are usually selected in such a way that they yield similar binding energies and charge radii as the experimental data. Sometimes a minimum distance between two arbitrary nucleons is required to give a more uniform initial phase-space distribution (IBL, IQMD-BNU, ImQMD). In some models (pBUU, CoMD, IQMD-SINAP), a frictional cooling method is used to reach a ground-state initialization. More information about the initialization of different codes used in the present work is given in Table. II and in the references listed in Table. I.

The density profiles at  $t = 0$  fm/c from BUU-type models and QMD-type models are shown in Fig. 1. These are averaged density distributions of the projectile and target over all the calculations requested in the homework (i.e., 10 runs with 100 TPs for BUU and 1000 events for QMD). The density distributions are obtained by folding the test particle positions with the width of the (test) particle as provided by the code practitioners, or by a default value of 1.5 fm. The initial phase-space distributions are seen to vary from code to code. BUU-type models (left panel) have a smaller dispersion, while QMD-type models (right panel) are more different from each other. AMD in its more quantum nature succeeds very well to produce good ground states and resembles the closest the Woods-Saxon distribution profile. AMD also exhibits an oscillatory behavior in the center similar to shell effects observed in Hartree-Fock calculations. The representation in Fig. 1 emphasizes the differences in the interior, while there are also considerable differences in the tail. To show this, the deviation values of  $\langle r^2 \rangle^{1/2}$  and  $\langle r^4 \rangle^{1/4}$  from that of the required Woods-Saxon distribution for each code are listed in Column 4 and 5 in Table II. The main difficulty in reproducing the given Woods-Saxon density profile is that the initialization depends on the implementation of individual codes and the shape of the test particles or wavepackets. Of course, differences in the initial momentum distributions are also important, especially when comparing observables related to the final momentum distributions, as in Sec. V C and V D. Initial momentum distributions are shown later (upper panels of Fig. 9).

From the above comparison, we learnt the different situations in the initializations between BUU and QMD approaches. In BUU, with the quasi-continuous distribution function for many test particles, it is not too difficult to obtain initial states with a reasonably smooth density and momentum profile. These initial states are usually also more stable, especially if they are calculated in a Thomas-Fermi or Hartree calculation using the same energy-density functionals as in the transport calculation, rather than prescribed as a density profile. For QMD approaches, with their larger fluctuations, the initially prepared states are less stable and many attempts are necessary to find stable initial states. Often criteria on the binding energy of the initialized nuclei and/or stochastic cooling are used additionally.

## B. Density Evolution

To check the stability of the initial configurations as described in the previous subsection, we examine the time evolution of radial density distributions of nuclei every 20 fm/c. Figures 2 and 3 show the corresponding density profile

as a function of radial distance for BUU-type and QMD-type models, respectively. Ideally, if the initial nuclei are stable, there should be no time dependence of the density distributions. Examples are GIBUU-Skyrme, pBUU, AMD, and CoMD codes, where the density profiles show stability within the simulation time of 140 fm/c. Generally, this requires special treatments such as phase-space constraint or extremely good Pauli blocking, because the transport models are not designed to calculate good ground states of a nucleus. A bubble-like configuration is formed initially in the IBL and possibly in the BLOB codes with the choice of the parameter set imposed by the homework. Such structure is not evident in any QMD codes. In other codes such as IBUU, RVUU, SMF, TuQMD, and IQMD-IMP, the radius of the nucleus oscillates like a giant monopole resonance. This is understandable as the given initial density distribution may not represent the ground state. In many QMD codes (IQMD-BNU, IQMD-IMP, IQMD-SINAP, and UrQMD), the nucleus evolves away from the initial density distribution (black lines) quickly and most relax into a reasonably stable configuration. Such instability seen for the initialized nuclei demonstrates the difficulty of imposing a common initial configuration to different codes. The different initial density distributions from all 18 codes shown in Fig. 1 illustrate that a common initialization in a code comparison is more involved than naively expected. The representation of the system with nucleons or with a quasi-continuous distribution function and the shape of the (test) particles are closely connected and affect the evolution and stability. The procedure chosen here to prescribe a common density profile of the initial nuclei is not optimal and often produces an initial configuration that is not stable. It may be more important to start with reasonably good ground states such that no spurious evolution affects the results. In this respect box calculations as discussed in Sec. VII for the future of this code comparison project may avoid this difficulty of the initialization.

## V. HEAVY-ION COLLISIONS AT $b = 7$ FM

In this section we present and discuss the comparison of the different transport codes when employed to simulate a heavy-ion collision. The impact parameter was chosen to be 7 fm, which corresponds to a reduced impact parameter of about 0.5. In such a reaction violent interactions take place and all aspects of a heavy-ion simulation are going to be important: the initialization of the system, the mean-field propagation, and the collision term with the collision probabilities and the Pauli blocking, thus allowing us to observe and understand the model dependencies. In doing so, one should also be able to observe many features of heavy-ion collisions, especially since in a simulation we have the advantage of being able to look into every aspect of the evolution.

We will look into the different aspects of a collision. In the first subsection, we discuss the density evolution of the reaction qualitatively in contour plots. In the second subsection, we look in detail into the action of the collision term with respect to two aspects, the probability of a NN scattering and the effect of Pauli blocking. We then discuss observables, which are commonly used in the comparison of a simulation with experiment, the rapidity distribution and the collective flow. The results are the average from all runs of the homework, and we do not show the statistical width of the results of each code, in order not to make the figures too crowded. As before, we group together BUU and QMD codes, respectively, in the figures. One expects and does in fact see that there are many similarities between the results of these two groups, but one also sees characteristic differences, associated with the different strategies of these codes as discussed in Sec. II.

### A. Density Evolution

The density contours in the  $x$ - $o$ - $z$  plane (i.e., the reaction plane with  $x$  the direction of the impact parameter and  $z$  the beam direction) in steps of 20 fm/c in Au+Au collisions at 100 AMeV are displayed in Figs. 4 and 5 for the BUU and QMD models, respectively. The contour plots give a good qualitative impression of the dynamical evolution in different models. The plots actually represent the average over all runs, i.e., 10 runs with 100 TPs in BUU and 1000 runs ("events") in QMD. This averaging smears out fluctuations, which are expected to be stronger in QMD models than in BUU models.

The general progression of a heavy-ion collision is exhibited in all models: the merging and maximum compression up to about 40 fm/c, the development of sideward flow from about 60 to 80 fm/c, and the formation and subsequent breaking of a neck at about 100 fm/c. From 100 fm/c onward, one observes the formation and evolution of the projectile- and target-like residues, which are clearly highly excited and develop their own dynamics. The final de-excitation of the excited fragments is not the subject of this comparison, but should be taken into account, if one wants to compare to experiment. In this collision, one could consider 140 fm/c as the freeze-out time, after which the de-excitation of the primary fragments is usually calculated with a statistical code.

Consistent with the density profiles of Fig. 1, we clearly see in the contour plots of Figs. 4 and 5, that the initial states in the different codes are rather different with more or less steep density profiles. It is interesting to see that

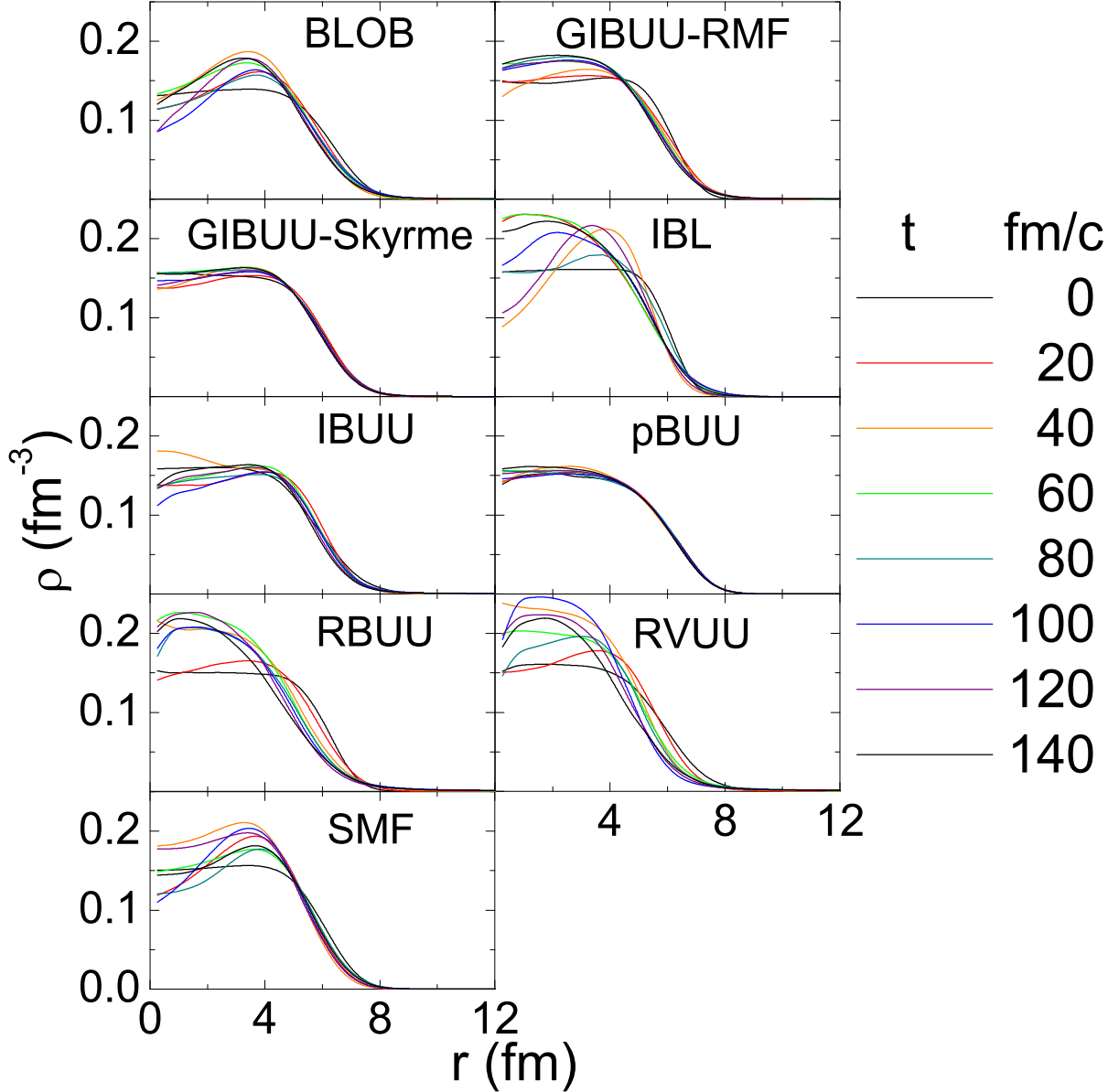


FIG. 2: (Color online) Time evolution of the density profiles in a single Au nucleus in steps of 20 fm/c (see legend for the explanation of different color lines) for BUU-type models at  $b = 20$  fm.

higher initial densities, which occur more often in QMD codes, lead to an earlier and stronger development of the high-density phase in a reaction. This supports the suggestion that differences in the initialization may actually lead to differences in the evolution and the physics observables and underscores the difficulty of code comparisons without identical initial states. The maximum density is reached by all models around 40 fm/c. The time span from 20 to 40 fm/c is very important for many observables, such as stopping, flow, and particle production, since in this interval most of the elementary collisions occur, as will be discussed in the next subsection.

One can see that here the evolution is characteristically different in BUU and QMD models. The density pattern is more detailed in BUU with distinctly compressed central zone and often normal density at the center of the residues. In QMD the density pattern appears more uniform, but this is primarily due to the averaging over many events. To demonstrate this, we show in Fig. 6 the density contour plots at the time of 100 fm/c for four different runs each generated by one BUU code (IBUU) with 100 TPs and by one QMD code (ImQMD-CIAE). The final states in the QMD model show a large amount of fragmentation. The difference in fragmentation patterns in Fig. 6 between BUU (left panels) and QMD (right panels) also reflects to which extent small structures can be generated by the different

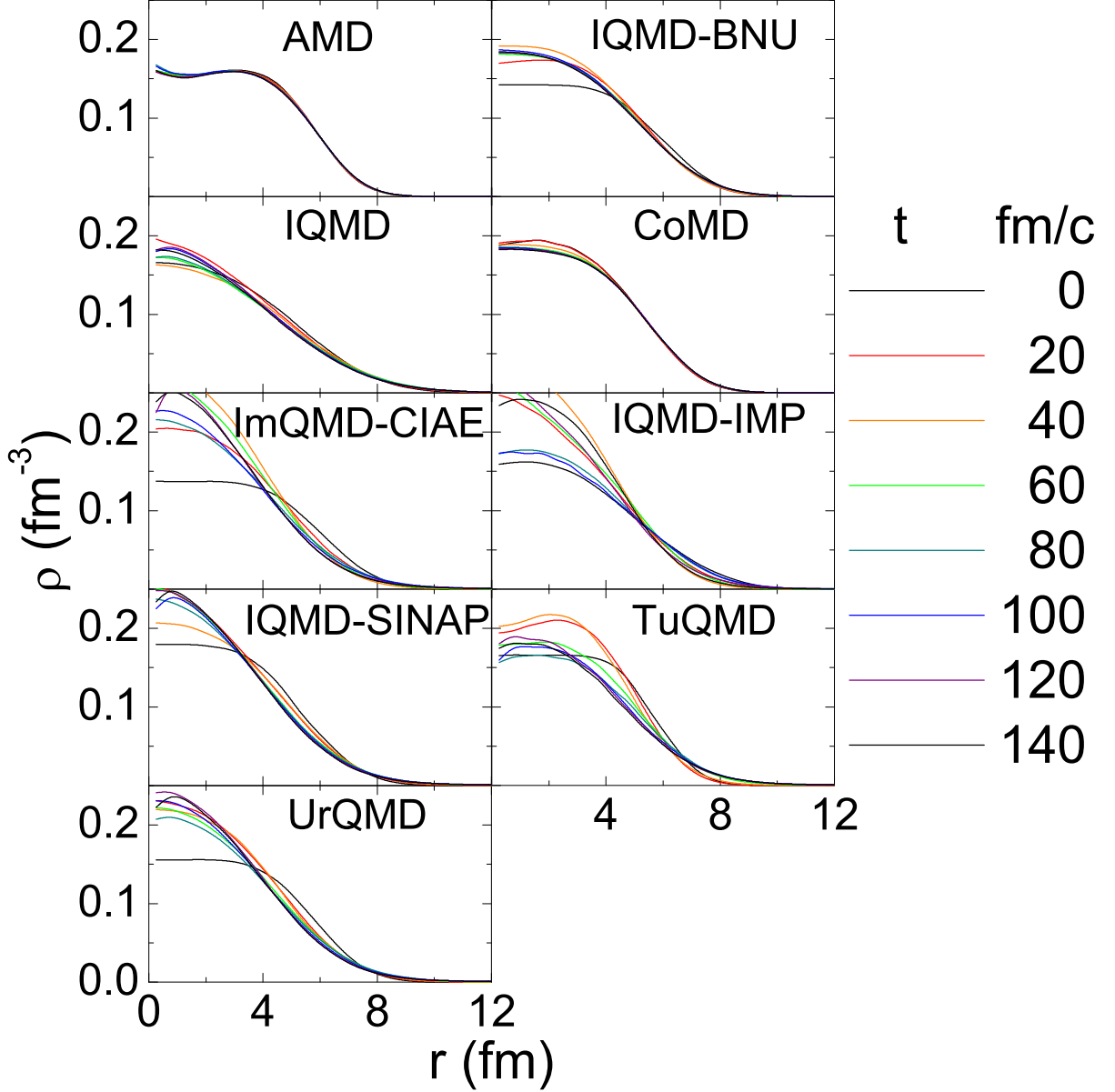


FIG. 3: (Color online) Same as Fig. 2 but for QMD-type models.

representation of the phase space by test particles or nucleons. In BUU these fine structures partly survive in the averaged distributions of Fig. 4. The similarity of the four runs also demonstrates the more deterministic nature of the BUU method. As discussed in Sec. II C, without introducing additional stochastic mechanisms (such as in BLOB or SMF), the fluctuation in BUU-type models depends on the test-particle numbers, and with infinite number of test particles the simulation leads to a deterministic solution of the BUU equation. For QMD-type models, the fragmentation character can be related to the width of the Gaussian wavepacket, and they are expected to show more fluctuations than in BUU-type models. A detailed study of the fluctuation and fragmentation patterns of different codes is planned in future efforts of this code comparison, as will be discussed below in the Outlook. It is thought that for the bulk one-body observables discussed here these will be of lesser importance, but they may already have an effect on the collision rates.

There are also differences in the evolution of the neck between 60 and 100 fm/c. In BUU the neck is usually fatter and stretches out farther. In the breaking of the neck fine structures (or even small fragments) appear. The residues are strongly deformed for a long time. In QMD the neck breaks faster and the residues rather quickly approach a spherical shape. Again these differences are mostly due to the averaging, since in single QMD events fragments are

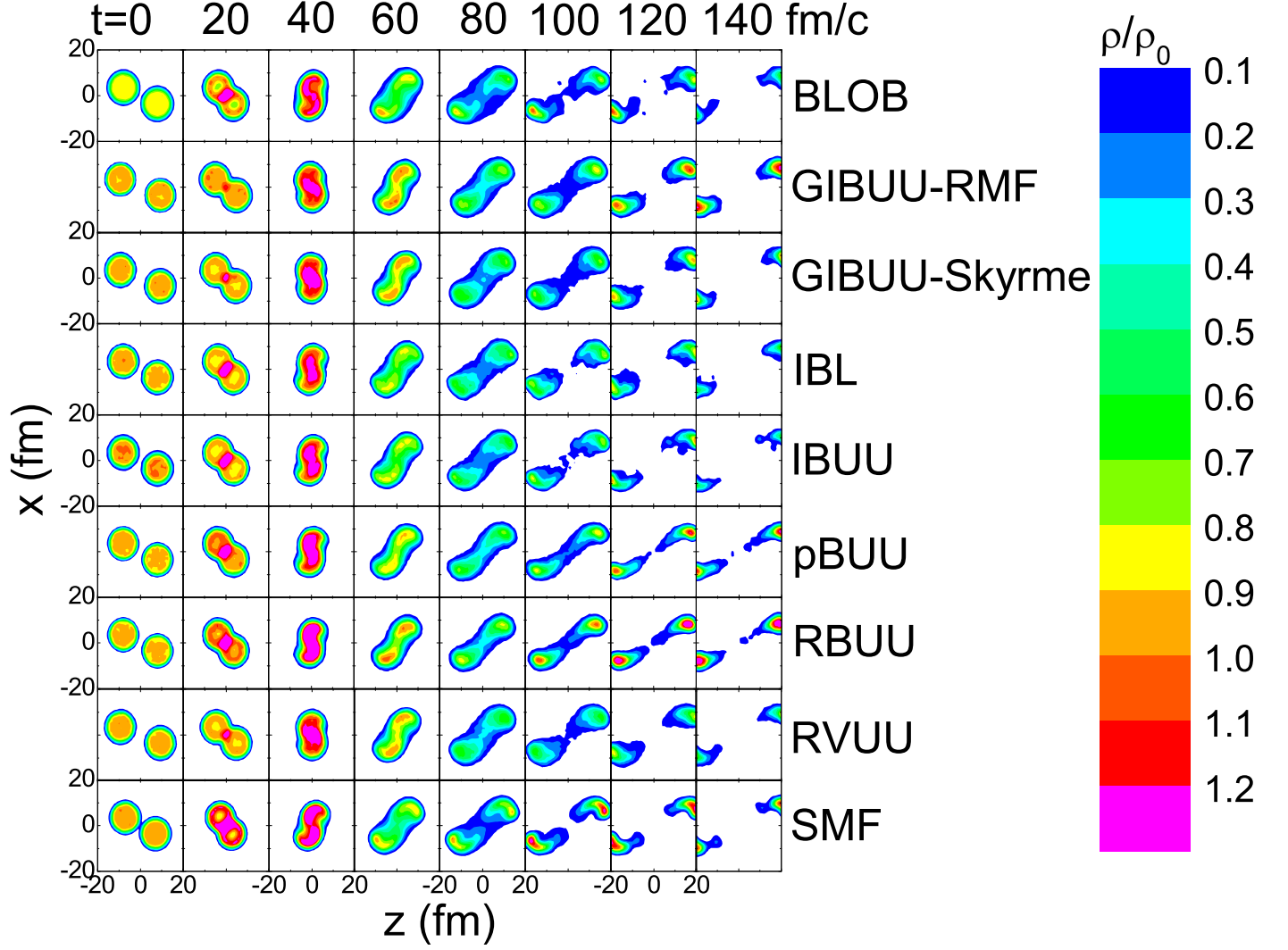


FIG. 4: (Color online) Average density contours in steps of 20 fm/c in Au+Au collisions at impact parameter  $b = 7$  fm and beam energy 100 AMeV from BUU-type models. This is for the B-Full mode that includes both mean-field potentials and nucleon-nucleon scatterings.

formed in the neck as shown in the right panels of Fig. 6.

Considering these differences, it will not be surprising that different codes will show differences in the collisional characteristics to be discussed in the next subsection, and in observables to be discussed in subsection C.

### B. Collision term

The collision term is the other important ingredient besides the mean field. As formulated in Eq. (2), it is highly non-linear in distributions and non-local in momentum, and therefore is simulated stochastically, as discussed in Sec. II. The collision term is crucial for the evolution of the simulation of a heavy-ion reaction, since it is the cause for energy dissipation. It is also the part of a simulation where different codes differ most in the implementation. It is therefore worthwhile to examine the collision rates in detail, even though these are not observables.

We have studied both the time evolution of the total collision rates and their distributions over energy. We show

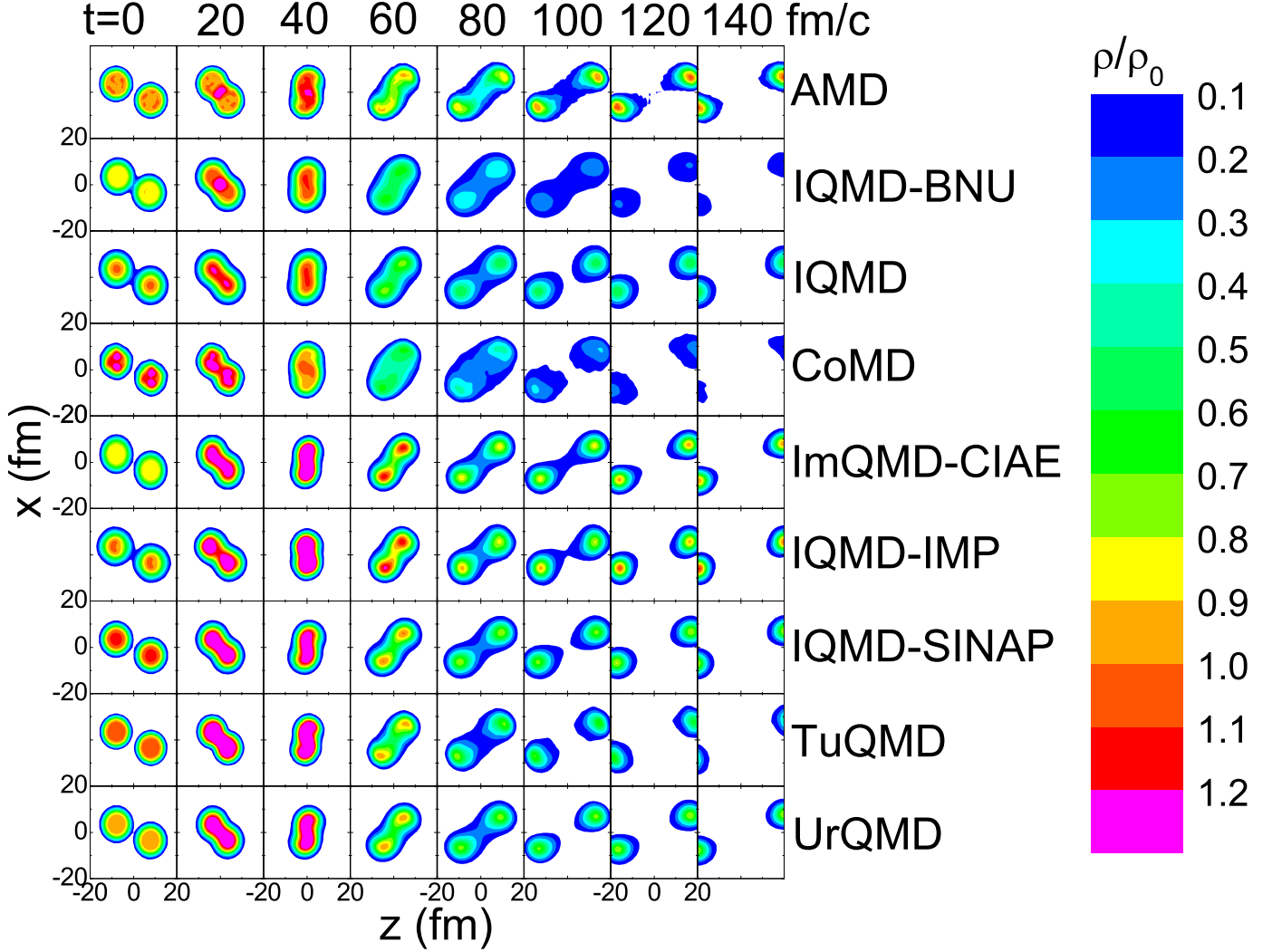


FIG. 5: (Color online) Same as Fig. 4 but from QMD-type models.

only the latter here, since they provide better physics insights. We note that the time evolution of the collision rates is closely linked to the density evolution, with the highest rates in the densest phases. They therefore also trace the density evolution shown in Figs. 4 and 5. For instance, one observes rise and fall in the collision rates when the residues oscillate.

The number of collisions per 100 keV bin are plotted for BUU and QMD codes in Figs. 7 and 8, respectively, as a function of the center-of-mass (CM) energy  $\sqrt{s}$  of the individual nucleon-nucleon collision. The arrangement of both figures is the same. In the left column we show the "attempted" collisions, which according to the definition in Sec. II are the collisions where the distance criterion (and in some cases additional criteria) are satisfied. The middle column shows the "successful" collisions, which are the attempted collisions (where the final state is not Pauli-blocked). The rightmost column shows the Pauli blocking factor, defined as  $1 - (\text{successful}/\text{attempted})$ . The upper and bottom rows show the B-Full and D-Full mode, respectively, i.e., a simulation with mean field and collisions at 100 and 400 AMeV, respectively. The middle row shows the B-Cascade mode, i.e., a simulation without the action of the mean field. Obviously we do not show the B-Vlasov mode, since there are no collisions there.

Generally we see the following behavior: in the NN frame we have the relation  $s = 4(m^{*2} + p^2)$ , where  $m^*$  is the

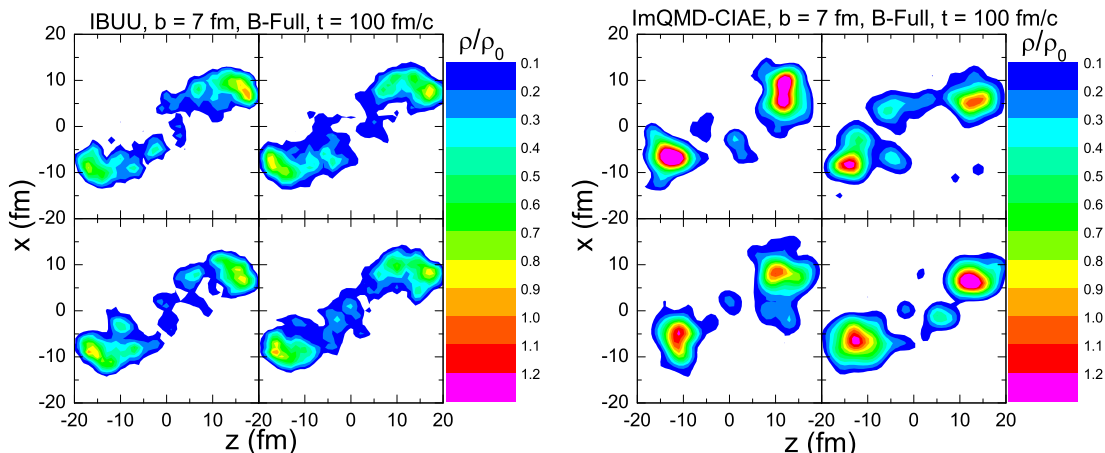


FIG. 6: (Color online) Density contours for 4 runs with 100 TPs per nucleon from IBUU (left) and four individual events from ImQMD-CIAE (right) out of the collisions displayed in Figs. 4 and 5 at  $t = 100$  fm/c.

effective mass and  $p$  is the modulus of the 3-momentum in the CM frame of the NN collision. The threshold with the prescribed free nucleon mass of 938 MeV is  $\sqrt{s} = 1.876$  GeV. In the figure this sharp cutoff is slightly smeared out due to the plotting procedure. For relativistic codes the effective Dirac mass and dressed momentum provided by the code authors were used in the analysis, compared with the results from the bare mass and momentum for non-relativistic codes.

The  $\sqrt{s}$  for a free NN collision is 1.925 and 2.066 GeV for an incident energy of 100 and 400 AMeV, respectively, and 1.894 GeV for particles at the Fermi momentum. In Figs. 7 and 8 it is seen that the peak energy for the maximum collision number is only approximately 1.9 GeV for both incident energies. By checking also the time evolution of the NN scattering number, we found that most of the collisions occur in the most compressed stage, when most of the nucleons are stopped to a large degree. However, the energy distribution has a long tail at higher CM energies, which is even more extended for 400 AMeV, as expected.

The number of collisions is considerably smaller in the Cascade mode, because here the nuclei disintegrate faster, due to the lack of mean field, resulting in lower densities. At 400 AMeV, the number is even smaller because of the faster disintegration of the system. Note the change of scale for the number of attempted collisions for the B-Cascade and D-Full modes.

The number of successful collisions is obviously lower than that of the attempted collisions. The shape of the energy distribution of the successful collisions looks similar to that of the attempted collisions, but this, in fact, is not quite so as shown by the blocking factors in the third column, which are not constant. The blocking factors are larger at lower energies, since the final states of softer collisions are more likely to be blocked due to the smaller phase space. The blocking is reduced for higher NN collision energies, since more of the phase space is free, particularly for the higher incident energy.

There are considerable differences in the implementation of the collision term in the different codes (see Table III). In some codes (IBL, IBUU, and IQMD-BNU) collisions start with a higher threshold than the free one. Here threshold is introduced to suppress very soft collisions, based on the argument that these are often spurious. In these codes the energy distributions are different from those without artificial collision threshold.

The distributions of the attempted collisions in the B-Cascade mode are rather similar between many codes both for BUU and QMD (but not so much for the successful collisions). This is what one expects as a consequence of no mean-field dynamics and the use of the same cross sections. Exceptions are the codes IBL, IBUU, AMD, ImQMD-CIAE, and IQMD-IMP probably due to different treatments of collision threshold or due to different initial density distributions.

The successful collisions are more important quantities in the Full modes, because they determine the energy dissipation. The collision numbers are higher in some cases for the relativistic codes (RBUU at 100 AMeV, RVUU at both energies, TuQMD at 400 AMeV, but not GIBUU-RMF) and also for IQMD-SINAP and ImQMD-CIAE. The peak of the energy distribution is shifted in some cases: to the lower side for BLOB, to the higher side for IBL, IBUU, and IQMD-BNU. In pBUU and IQMD the total number of successful collisions is relatively low, and also for AMD and CoMD at the higher incident energy. The last observation is understood for AMD which treats a NN collision as that of two phase-space wavepackets. Since the collision probability is proportional to the relative velocity between



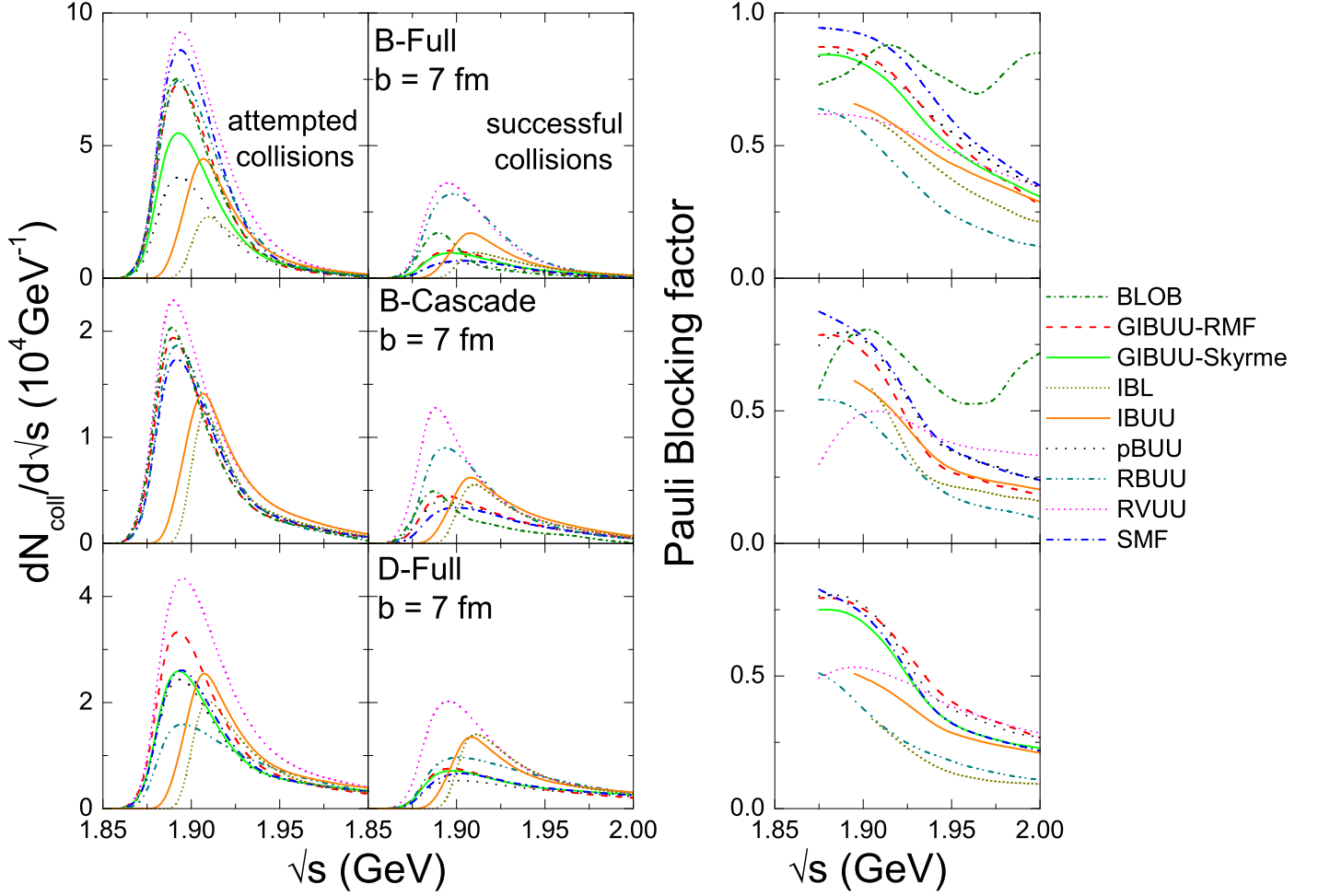


FIG. 7: (Color online) Center-of-mass energy dependence of nucleon-nucleon attempted (left) and successful (middle) scattering numbers as well as the Pauli blocking factors (right) for the B-Full mode (top), the B-Cascade mode (middle) both at 100 AMeV, and the D-Full (bottom) mode at 400 AMeV at impact parameter  $b = 7$  fm from BUU-type models.

the centroids without velocity fluctuation, the number of collisions is smaller than those in other models at lower  $\sqrt{s}$ . A similar situation might exist for CoMD, where particularly the collision numbers are much smaller at higher  $\sqrt{s}$ . A contrary case exists for the relativistic QMD code TuQMD, where the number of collisions is typical at 100 AMeV, but higher at 400 AMeV.

The Pauli blocking factors in the third column show that, to what extent the differences in the successful collisions are due to the blocking. Generally the blocking factors are considerably different between codes but the trends are similar, i.e., they have similar shapes for different codes, signifying that the blocking behavior does not depend very much on the CM energy of the NN scattering. The blocking factors tend to converge better at the higher NN scattering energies, especially at the higher incident energy of 400 AMeV (with BLOB data not available). This is expected since in high-energy collisions the density evolution of the collision matters less. There are some exceptions in the blocking factors. CoMD has a very different energy dependence of the blocking factor. This behavior reflects phase-space correlations produced in the initial configurations, which inhibit collisions with relative momenta near the Fermi momentum (inner particles), but not so much at the surface (low relative momenta) because of lower densities.

In summary, there are considerable differences in the behavior of the collision terms between different codes, which, however, tend to diminish at higher incident energies. Aside from the different initializations as discussed earlier, these differences or similarities are most likely behind the differences and similarities for the behavior of the observables, which will be discussed in the next two subsections.

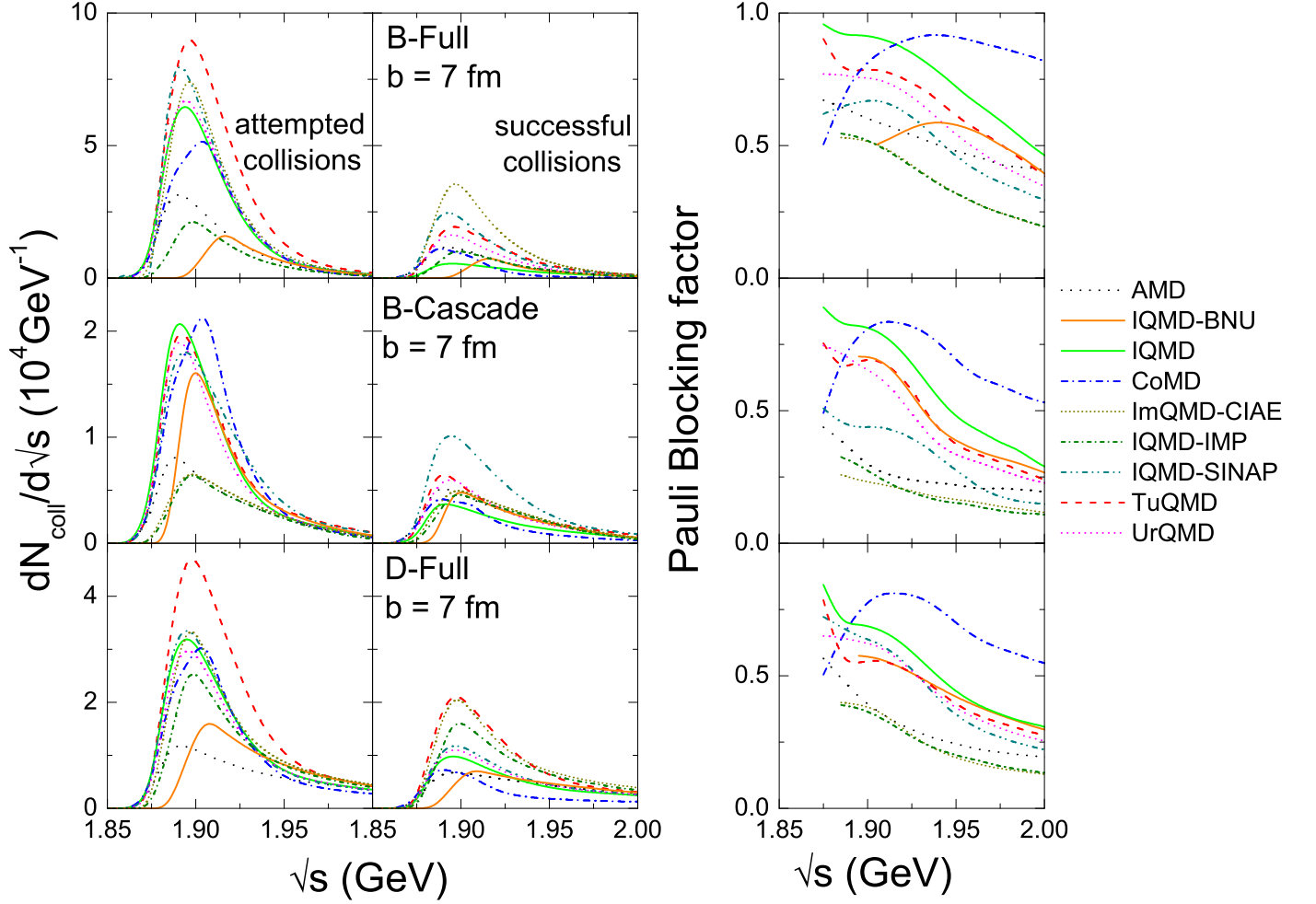


FIG. 8: (Color online) Same as Fig. 7 but from QMD-type models.

### C. Rapidity distributions

A rapidity distribution characterizes the distribution of particles along the beam axis in a Lorentz invariant manner. The distributions are usually displayed relative to the beam rapidity, so that projectile and target sit at  $y/y_{beam} = \pm 1$  in the CM frame, respectively. A rapidity distribution tests the stopping of the nucleons in a heavy-ion collision and is an important basic observable.

In Fig. 9 we show the rapidity distributions for the B-mode (100 AMeV) calculation from BUU codes on the left and from QMD codes on the right. The first row shows the initial distributions and the next rows are the final distributions for the Vlasov, Cascade, and Full modes, respectively. In Fig. 10 we compare the results of the Full mode for 100 and 400 AMeV incident energy. The initial distributions exhibit a double-humped structure. These are the expected superposition of the initial target and projectile distributions boosted to  $\pm$ beam rapidity as mentioned. In the Vlasov mode, the peaks in final distributions are moved somewhat inward to midrapidity, corresponding to a braking of the longitudinal velocity due to the action of the Coulomb and nuclear mean fields, and to the collective deflection of the motion in transverse direction (see the next subsection where this is shown in more details). The NN scatterings lead to a filling of the midrapidity distribution in the B-Cascade mode, since they convert the longitudinal into random momentum (especially for an isotropic cross section used here). The amount of filling, called stopping and the opposite behavior called transparency, should depend on the NN scatterings. The Full mode combines both effects. Generally the peaks of the Full mode are between those of the Vlasov and Cascade distributions, but the exact shape can be different depending on the code. In Fig. 10 one sees that the stopping is weaker at the higher incident energy, correlating with the smaller number of collisions, already seen in Figs. 7 and 8.

As shown in Fig. 1, the initial rapidity distributions for all BUU codes are rather similar, as was intended. We

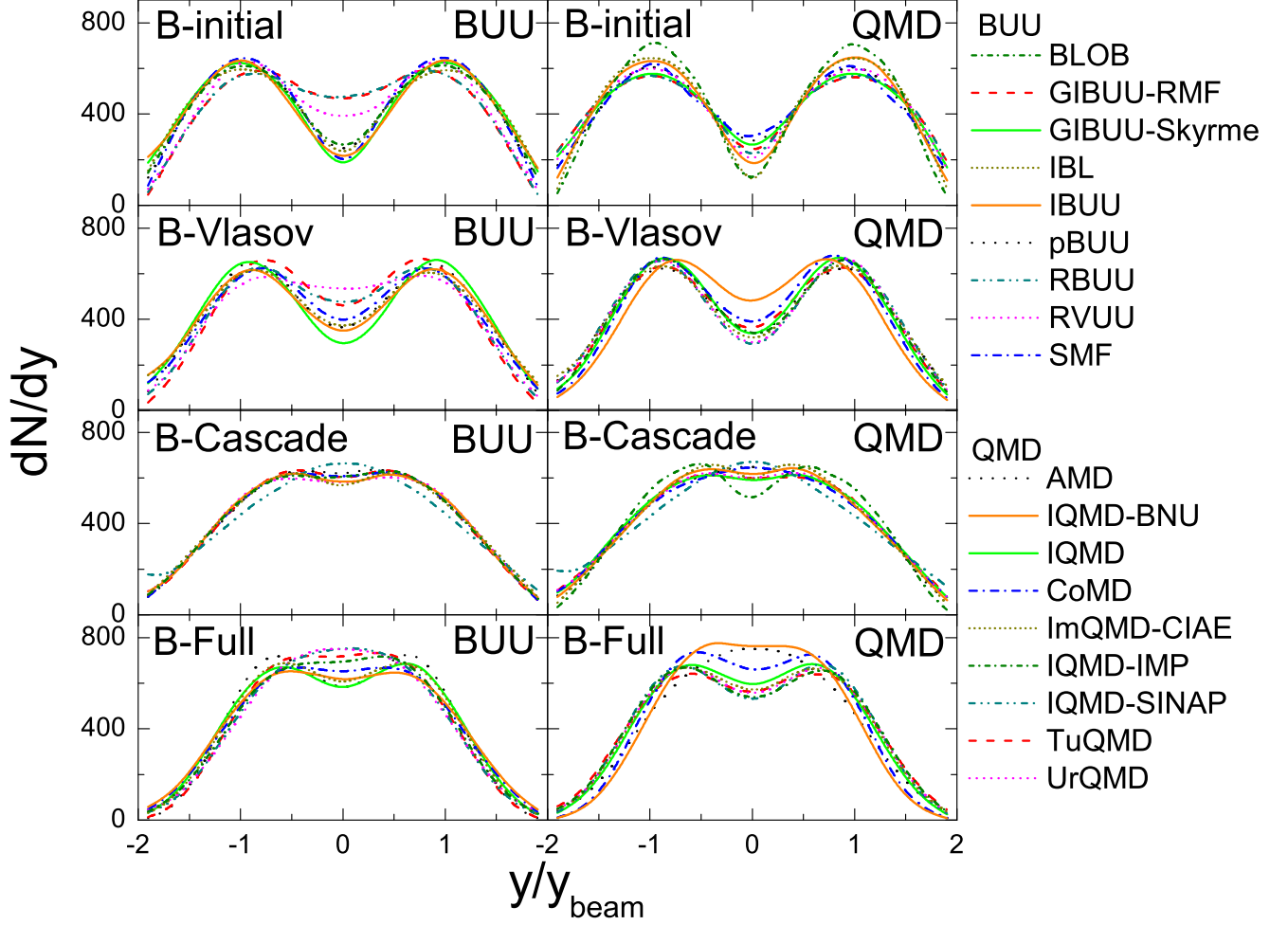


FIG. 9: (Color online) Initial rapidity distributions (top panels) at the beam energy of 100 AMeV and final rapidity distributions for the B-Vlasov mode (next panels down), the B-Cascade mode (next panels down), and the B-Full model (bottom panels) at impact parameter  $b = 7$  fm from BUU-type (left panels) and QMD-type (right panels) models.

note that for the relativistic BUU codes (GIBUU-RMF, RBUU, and RVUU), the Dirac effective mass and the dressed momentum provided by the code practitioners are used to calculate the rapidity, which leads to a flatter rapidity distribution compared with those from non-relativistic codes. There are, however, larger differences in the QMD codes, correlating with the larger spread in the initial density profiles seen in Fig. 1.

One would expect that the rapidity distribution for the B-Vlasov mode should be similar for all the codes, but this is not completely true as shown in the second row of Fig. 9, most likely due to the different initial density and momentum distributions.

In the B-Cascade mode the results are remarkably similar for all BUU codes, but larger differences appear for the QMD codes. One can relate these differences to those in the successful collisions in the Cascade mode in Figs. 7 and 8, which explains some (but not all) of the different behaviors. The large stopping in the RBUU code is correlated with the large collision numbers in Fig. 7 (but this is not the case for the large collision numbers for RVUU). For the IQMD-SINAP code there is a clear correlation between the almost complete stopping with the large number of collisions. For AMD and CoMD the stopping is relatively strong, even though the collision numbers are not particularly high. For IQMD-IMP the larger transparency is related to the somewhat lower collision numbers.

In the Full mode we see the competition between the mean field and the NN scatterings. In BUU models the rather similar Cascade distribution are split up by the more different Vlasov results, and the other way around for QMD

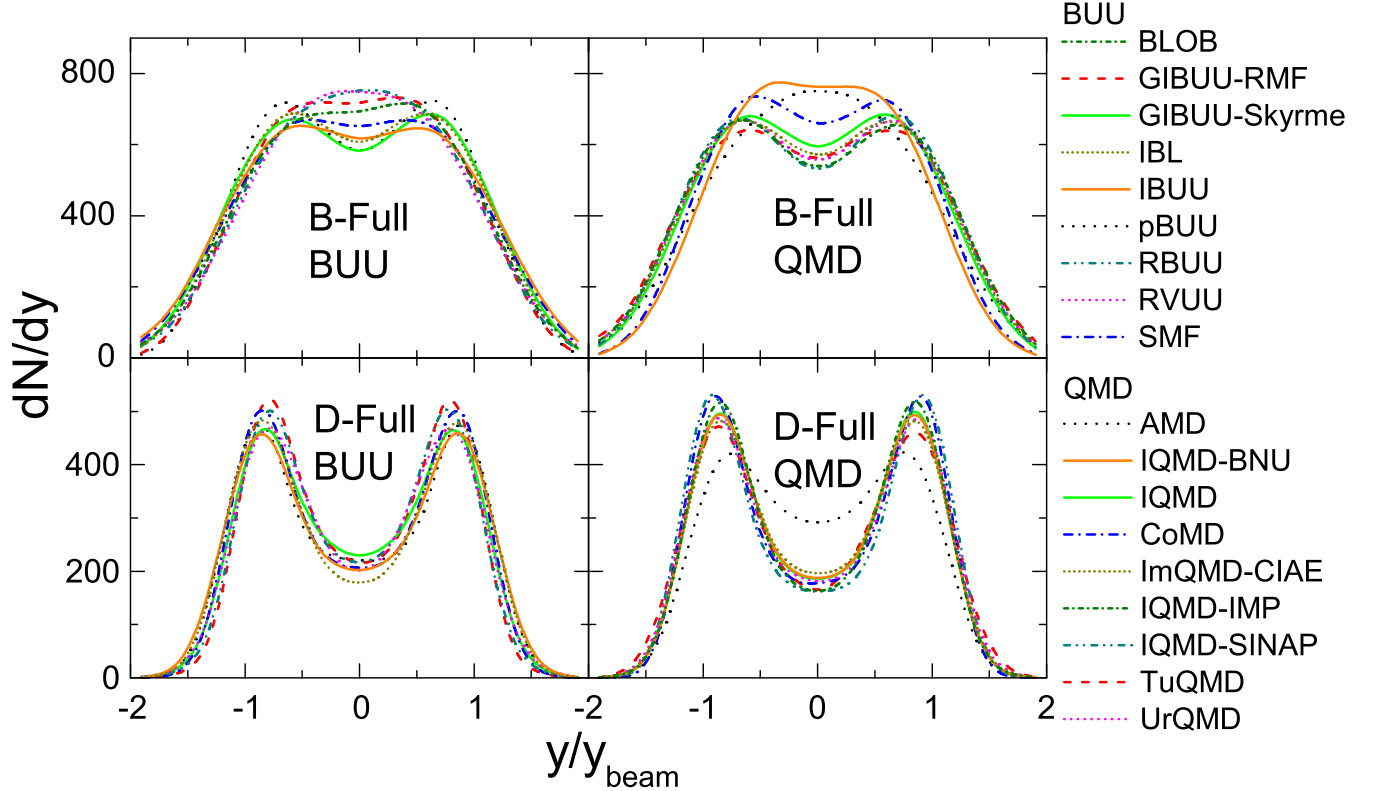


FIG. 10: (Color online) Rapidity distributions at  $b = 7$  fm for the B-Full (top panels) and D-Full (bottom panels) mode from BUU-type (left panels) and QMD-type (right panels) models.

codes. For the Full mode in both types of codes there are considerable differences. There is again a correspondence between the stopping and the number of successful collisions in the Full mode. The relativistic BUU codes have stronger stopping, which might be due to their initial rapidity distribution. For CoMD the strong stopping from the full calculation is related to its initial rapidity distribution, while for IQMD-BNU the large deflection in the Vlasov mode seems to dominate also in the Full mode.

In Fig. 10 the similarity of the rapidity distribution at the higher incident energy of 400 AMeV for almost all codes is remarkable. In the case of AMD, probably too many nucleons participate in violent collisions, due to the insufficient precision of the physical-coordinate representation discussed in Ref. [27], which overestimates the radius of the Au nucleus. The similarity of the rapidity distributions at 400 AMeV appears in spite of the differences in the collision spectra. The reason may be that the stopping at higher incident energies is dominated by the NN scatterings and particularly those at higher CM energies, where almost all codes converge rather well, as seen in Figs. 7 and 8. Thus stopping is a rather robust observable between different codes at high incident energies.

#### D. Anisotropic collective flow

Given the anisotropy of the evolving density in Figs. 4 and 5, one can infer that, in a collision with finite impact parameter, an anisotropy in the collective momentum distribution develops. This collective flow is usually quantified in terms of a Fourier series expansion of the dependence of the yield on the azimuthal angle

$$N(\phi; y, p_T) = N_0 \left[ 1 + 2 \sum_n v_n(y, p_T) \cos(n\phi) \right]. \quad (9)$$

The first two coefficients in this expansion ( $n = 1$  and  $2$ ) are called the directed and elliptic flow, respectively. They are functions of rapidity  $y$  and transverse flow  $p_T$  and are important observables in heavy-ion collisions. They are of particular interest at midrapidity, where particles and clusters come more directly from the compressed region and

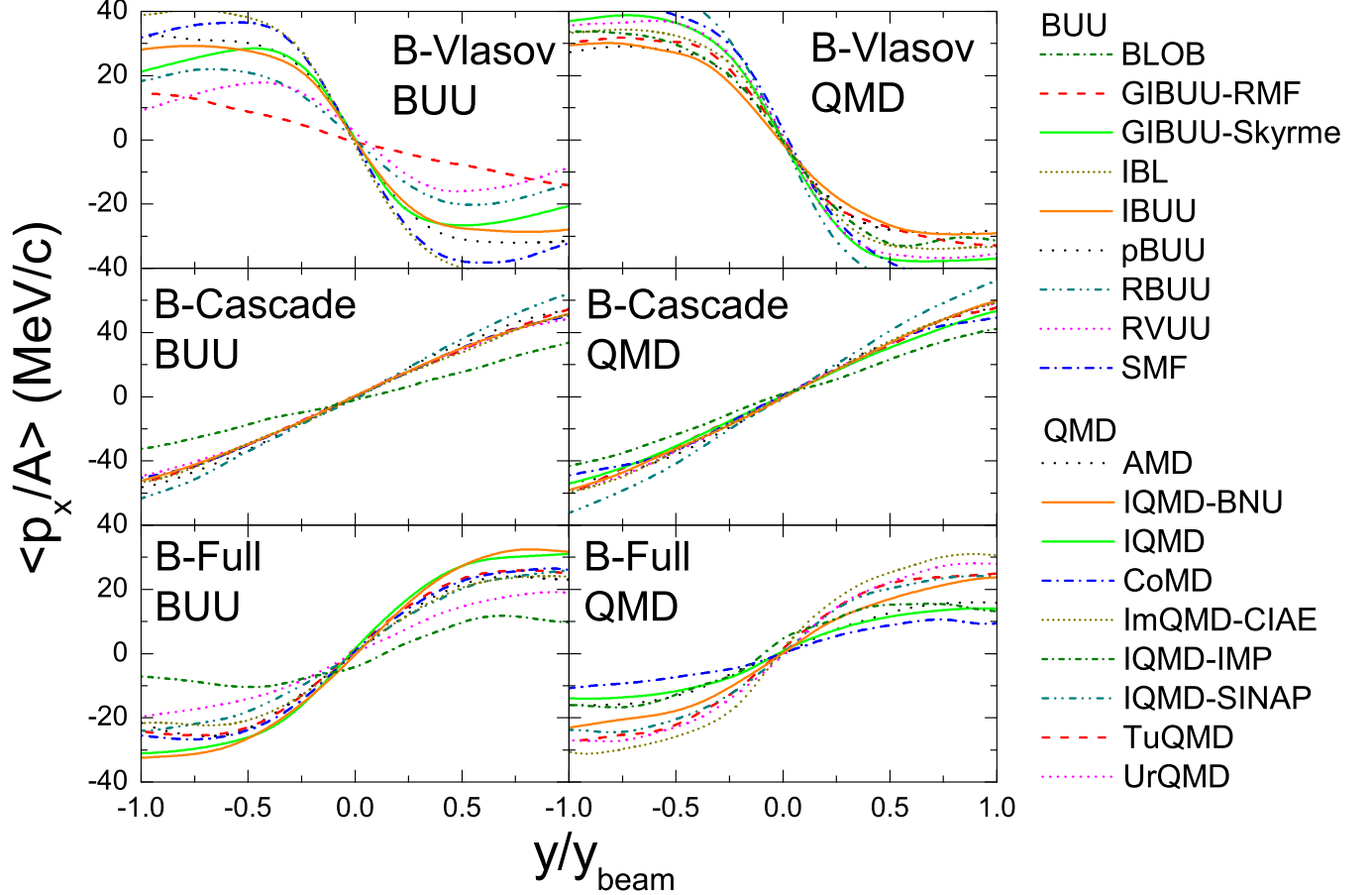


FIG. 11: (Color online) Transverse flow as a function of reduced rapidity for the B-Vlasov mode (top panels), the B-Cascade mode (middle panels), and the B-Full mode (bottom panels) at  $b = 7$  fm from BUU-type (left panels) and QMD-type (right panels) models.

are therefore of interest in the determination of the high-density EoS. The flow is determined from both the mean field and NN scatterings, with the relative importance depending on the incident energy. Here we concentrate on the transverse flow, or rather on the average in-plane flow  $\langle p_x/A \rangle$ , which is closely related to the directed flow defined as  $v_1 = \langle p_x/p_T \rangle$ . We do not show the elliptic flow, normally considered at midrapidity, since the statistics in our calculations was rather low in the midrapidity region.

In Fig. 11 we show the transverse flow per nucleon as a function of the reduced rapidity  $y_{red} = y/y_{beam}$  in the CM frame for the B-mode calculation from BUU (left) and QMD (right) codes. The results for Vlasov, Cascade, and Full modes are shown in the top, middle, and bottom rows, respectively. In Fig. 12 we compare results from the full calculation for the B- and D-modes (100 and 400 AMeV). Because of the above arguments, the slope of the transverse flow at midrapidity, often simply called the flow, is of particular interest. The values of the flow for the full calculations from a linear fit in the range  $|y_{red}| < 0.38$  are plotted in Fig. 13. The error bars shown are the fitting uncertainties without taking into account the statistical error of the individual data points. The rapidity range is chosen to reflect the linear slope region around midrapidity since results from most codes exhibit an S-shaped curve. Due to symmetry, the transverse flow in Figs. 11 and 12 should be zero for  $y = 0$ , as is seen in most models. For BLOB the failure to show this is related to the effectively lower statistics than for other BUU models, as discussed in Sec. II C, and correspondingly a larger statistical error.

The transverse flow results from a competition between the mean field and the scattering terms. Above the Coulomb barrier the mean field is attractive for some range of energies, which leads to negative deflection angles, and thus to a negative slope at midrapidity for the transverse flow, as seen for the B-Vlasov calculations in Fig. 11. The NN scatterings act repulsively and lead to a positive slope as seen for the B-Cascade mode. The energy where the two effects just cancel each other is called the balance energy. We see, in the B-Full mode, that at 100 AMeV we are somewhat above the balance energy. The slope is positive, but smaller than that in the Cascade mode (note the

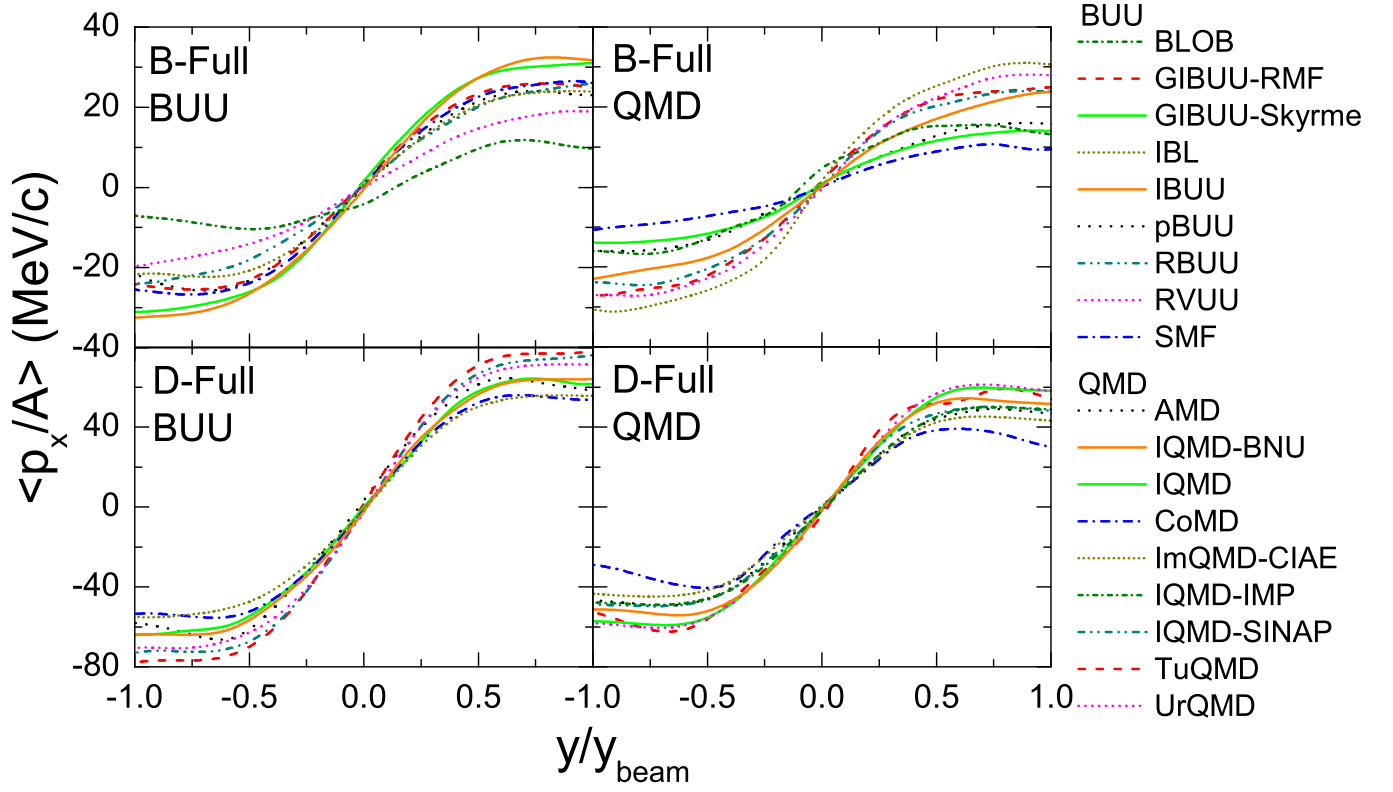


FIG. 12: (Color online) Transverse flow as a function of reduced rapidity for the B-Full mode (100 AMeV) and D-Full mode (400 AMeV) at  $b = 7$  fm from BUU-type (left) and QMD-type (right) models.

change of scale). One should note that different densities and density profiles are reached in Cascade, Vlasov, and Full modes, and thus quantitatively the effects are not directly comparable. At 400 AMeV the slopes in the full calculation (Fig. 12) are much larger. At this energy also the mean field acts repulsively (not illustrated). From these considerations one should expect a correlation between the flow and the rapidity distribution (Fig. 9), both in B-Vlasov and B-Cascade modes. For the Full mode this is less clear because of different effects competing. Indeed, one can observe such a correlation in some cases. Thus, in B-Vlasov mode RVUU and RBUU show a weak flow and a strong stopping, while the opposite is true for IBUU. In B-Cascade mode, however, IQMD-SINAP yields a large flow and a strong stopping, while the opposite is true for IQMD-IMP. But in other cases the correlations are not so clear. With increasing incident energy there is a stronger flow but a weaker stopping, because the competition of the contributions from the mean field and the NN scatterings to the flow changes.

For the B-Full mode the spread of the flow is considerable, as seen in Fig. 13, for both BUU and QMD models, which scatter about a common value of around 50 MeV/c. The low value observed in the BLOB case is related to the fact that this model includes fluctuations in the treatment of the collision integral, leading to a stronger fragmentation. At the higher incident energy the results for the transverse flow are visually closer. By assuming a systematic error of 3% for the transverse flow results besides the fitting error, we obtain the mean flow of  $51 \pm 11$  MeV/c at 100 AMeV and  $143 \pm 19$  MeV/c at 400 AMeV for the BUU codes and  $45 \pm 13$  MeV/c at 100 AMeV and  $116 \pm 12$  MeV/c at 400 AMeV for the QMD codes. The uncertainties reflect the standard deviations, which are similar in magnitude but relatively increase by about a factor of two, by comparing those at 400 AMeV with those at 100 AMeV. The results for BUU and QMD codes overlap within their error bars, but it seems that QMD models give a systematically smaller flow, which at 400 AMeV amounts to about 15%. One may conclude that flow is a robust observable with uncertainties from the simulations of around 13% at 400 AMeV. At the lower energy of 100 AMeV the uncertainties increase to about 30%.

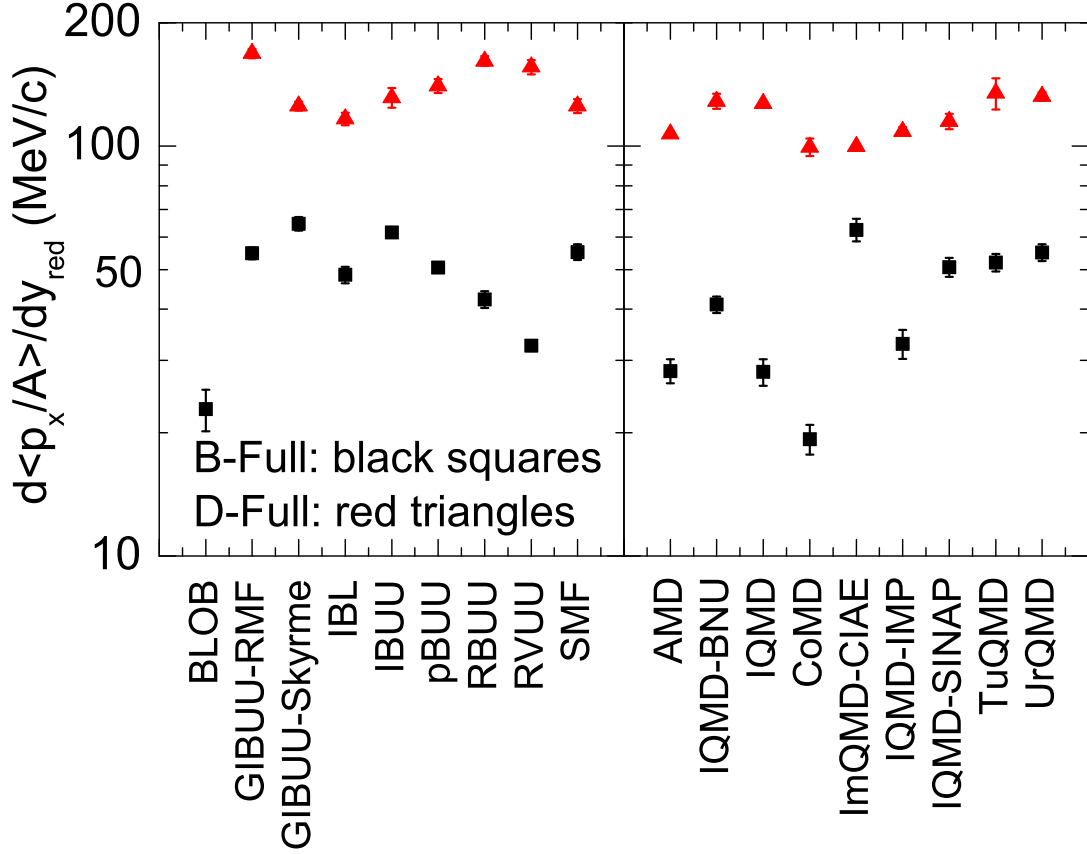


FIG. 13: Slope parameters of the transverse flow of 9 BUU-type (left) and 9 QMD-type (right) models from the B-Full mode (black squares) and D-Full mode (red triangles). The error bars are the fitting uncertainties. Where they are not seen they are smaller than the symbols.

## VI. DISCUSSION

Transport theories, in particular the BUU and QMD approaches, have been widely used in extracting physics information from heavy-ion collisions. However, because of the complexity of these theories, the corresponding simulations involve many choices and strategies. In this paper we have studied the robustness of the predictions from different transport simulation codes under controlled conditions of identical physics input and with as close as possible initial conditions, in order to obtain an estimate of the spread of the results.

In this comparison we find a considerable spread of results from different codes, which is larger at the lower incident energy. Since the philosophies of BUU and QMD approaches are different, e.g., fluctuations and correlations are treated differently, one cannot expect to completely eliminate the difference between the two approaches, but it is reassuring to see that similar results are obtained. While we do not attempt to validate different codes, we try to understand outliers with the help of the code authors where possible. The range of results found in this comparison gives for the first time an estimate of a benchmark for transport codes in these energy regions. One goal of the project is to improve these benchmarks, by investigating what causes the diverse results, and to identify the best strategies and methods to simulate the transport equations. In the absence of complete agreement, the aim of the project is to bring about theoretical uncertainties of less than 10%, which are typically achieved in experiments, so that comparisons of transport results with experimental data become more meaningful and robust.

One should consider the spread of the predictions, such as those shown in Fig. 13 and earlier figures, as a kind of systematic theoretical error of transport simulations, i.e., if another code were used to interpret the same experimental data, a different conclusion within this systematic uncertainty should be expected. Agreement of a simulation with an experimental observable alone may not serve as validation that the extracted physical parameters are reliable, because the variation of physical parameters could be compensated by strategies in the simulation. Of course, such a compensation is less likely, if a code is able to describe with the same physical input different observables at different

energies or different impact parameters.

Over the years, a large amount of the experimental data has been obtained in the extended Fermi energy domain from about 35 to 150 AMeV, including data on isotope yields [57–62] and on isospin diffusion [63], which at present have been most widely used for the determination of the symmetry energy at subsaturation densities. Our results seem to indicate that the robustness of the predictions may be reduced in this energy region, which is particularly sensitive because of competing effects of the mean field and the NN collisions on the observables and because of the importance of cluster formation. This is consistent with different conclusions reached in the transport simulation analyses [64–69]. Understanding and improving the predictions here is particularly important and should be undertaken in the future.

## VII. CONCLUSION AND OUTLOOK

The goal of this code comparison project is to determine and ultimately reduce the model uncertainties, in order to extract model-independent information on nuclear interactions from heavy-ion experiments. Based on 9 BUU-type models and 9 QMD-type models, we have compared the initialization, stability of the initial configuration, the number of attempted and successful collisions, and the effects of the mean field and collision terms, on the rapidity distribution and anisotropic collective flows in Au+Au collisions at beam energies of 100 and 400 AMeV. Although there is still considerable model dependence that needs to be further understood, we have learned some useful lessons from the comparison. We have found that the results from BUU and QMD approaches are essentially similar for the quantities compared here. The differences in the collision strategies are less important at higher incident energies as a result of weaker effects from initialization and Pauli blocking, and consequently the robustness of the predictions is higher. For the flow observables, we find uncertainties from code dependence of about 30% at 100 AMeV and 13% at 400 AMeV.

The divergence in the results of different codes very likely originates from several sources: Firstly, the initialization of the colliding nuclei is found to be rather different despite attempts to use a prescribed initial density profile. This seems to lead to differences in the evolution. Here an initialization based on approximate ground states consistent with the employed mean fields should improve the comparison. Secondly, from simulations with mean-field potentials only and with nucleon-nucleon scatterings only at 100 AMeV, the results for the attempted collisions and for the Pauli blocking factors show considerable differences in different codes. Some of these differences are due to different physically motivated strategies, which were not prescribed in this comparison, but left as in the normal usage of the code. This part of the transport simulations should be critically assessed in future comparisons.

In heavy-ion collisions many effects are closely intermingled: the density evolution, the collision probabilities and their Pauli blocking, the collective flows, and the fragmentation and clusterization. To understand these different factors better, it is advantageous to test them separately as much as possible. Therefore as a follow-up to the present work, plans are being made to compare simulations from different codes for a system of infinite nuclear matter, i.e., a calculation in a box with periodic boundary conditions. Here the initialization should not be problematic, the overall density is a constant, and the energy conservation should be strictly obeyed. For many quantities, such as the collision rates, exact analytic limits are available, and thus one may test the thermodynamic consistency of the codes, and disentangle better the effects of the mean field and those of the nucleon-nucleon scatterings. The results from such comparisons could establish important benchmarks in understanding transport simulations of heavy-ion collisions. Another future direction will be to compare more complicated, but in practice very important aspects of heavy-ion reactions, such as momentum and isospin dependence of the mean field, isospin transport, clusterization and fragmentation, and particle production.

## Acknowledgments

JX acknowledges support from the Major State Basic Research Development Program (973 Program) of China under Contract No. 2015CB856904 and No. 2014CB845401, the National Natural Science Foundation of China under Grant No. 11475243 and No. 11421505, the "100-Talent Plan" of Shanghai Institute of Applied Physics under Grant No. Y290061011 and No. Y526011011 from the Chinese Academy of Sciences, the Shanghai Key Laboratory of Particle Physics and Cosmology under Grant No. 15DZ2272100, and the "Shanghai Pujiang Program" under Grant No. 13PJ1410600. LWC acknowledges the Major State Basic Research Development Program (973 Program) in China under Contract No. 2013CB834405 and No. 2015CB856904, the National Natural Science Foundation of China under Grant No. 11275125 and No. 11135011, the "Shu Guang" project supported by Shanghai Municipal Education Commission and Shanghai Education Development Foundation, the Program for Professor of Special Appointment (Eastern Scholar) at Shanghai Institutions of Higher Learning, and the Science and Technology Commission of Shanghai Municipality (11DZ2260700). MBT acknowledges support from the USA National Science Foundation Grants No. PHY-1102511 and travel support from CUSTIPEN (China-US Theory Institute for Physics with Exotic Nuclei) under



the US Department of Energy Grant No. DE-FG02-13ER42025. HHW acknowledges support from the DFG Cluster of Excellence *Origin and Structure of the Universe*, Germany. YXZ acknowledges the supports from the National Natural Science Foundation of China under Grant No. 11475262 and the National Key Basic Research Development Program of China under Grant No. 2013CB834404. KK and YK acknowledge the supports from the Rare Isotope Science Project of Institute for Basic Science funded by the Ministry of Science, ICT and Future Planning and the National Research Foundation of Korea (2013M7A1A1075764). CMK acknowledges support by the Welch Foundation under Grant No. A-1358. BAL is supported in part by the U.S. National Science Foundation under Grant No. PHY-1068022, the U.S. Department of Energys Office of Science under Award No. de-sc0013702, and the National Natural Science Foundation of China under Grant No. 11320101004. AO acknowledges support from JSPS KAKENHI Grant No. 24105008. PD acknowledges support from the USA National Science Foundation Grant No. PHY-1510971. YJW and QFL acknowledge support by the National Natural Science Foundation of China under Grant Nos. 11505057, 11547312, and 11375062. GQZ acknowledges support by the National Natural Science Foundation of China under Grant No. 11205230. The authors would like to thank all the participants of the Transport 2014 workshop for their enthusiasm, support, and encouragement for the code comparison project. In particular, we would like to thank Zhigang Xiao, Yvonne Leifels, and Li Ou for their great help in leading stimulating discussion sessions during the workshop, and Joe Natowitz for careful reading of the manuscript and providing valuable comments. The writing committee (consisting mainly of the first 5 authors) would like to acknowledge the support and the excellent hospitality for their writing sessions at the Jagiellonian University, Cracow, Poland, and at Shanghai Institute of Applied Physics, Shanghai, China.

- 
- [1] G. F Bertsch, H. Kruse, and S. Das Gupta, *Phys. Rev. C* **29**, 673 (1984).  
[2] H. Kruse, B. V. Jacak, J. J. Molitoris *et al.*, *Phys. Rev. C* **31**, 1770 (1985).  
[3] J. Aichelin, *Phys. Rev.* **33**, 537 (1986).  
[4] A. Le Fevre, Y. Leifels, W. Reisdorf *et al.*, *Nucl. Phys. A* **945**, 112 (2016).  
[5] J. Aichelin and C. M. Ko, *Phys. Rev. Lett.* **55**, 2661 (1985); C. Fuchs, A. Faessler, E. Zabrodin *et al.*, *Phys. Rev. Lett.* **86**, 1974 (2001).  
[6] P. Danielewicz, R. Lacey, and W. G. Lynch, *Science* **298**, 1592 (2002).  
[7] C. Fuchs and H. H. Wolter, *Eur. Phys. Jour. A* **30**, 5 (2006).  
[8] V. Baran, M. Colonna, V. Greco *et al.*, *Phys. Rep.* **410**, 335 (2005).  
[9] A. W. Steiner, M. Prakash, J. M. Lattimer *et al.*, *Phys. Rep.* **411**, 325 (2005).  
[10] J. M. Lattimer and M. Prakash, *Phys. Rep.* **442**, 109 (2007).  
[11] B. A. Li, L. W. Chen, and C. M. Ko, *Phys. Rep.* **464**, 113 (2008).  
[12] M. B. Tsang, J. R. Stone, F. Camera *et al.*, *Phys. Rev. C* **86**, 015803 (2012).  
[13] J. M. Lattimer, *Annu. Rev. Nucl. Part. Sci.* **62**, 485 (2012).  
[14] C. J. Horowitz, E. F. Brown, Y. Kim *et al.*, *J. Phys. G* **41**, 093001 (2014).  
[15] B. A. Li, A. Ramos, G. Verde *et al.*, eds. *Topical Issue on Nuclear Symmetry Energy*, *Eur. Phys. Jour. A* **50**, 9 (2014).  
[16] E. E. Kolomeitsev, C. Hartnack, H. W. Barz *et al.*, *J. Phys. G* **31**, S741 (2005).  
[17] Workshop website: <http://www.physics.sjtu.edu.cn/hic2014/>  
[18] The results from ImQMD-GXNU from Ning Wang and Jun-Long Tian are not included in the comparison as this code is developed mainly for very low-energy reactions (< 50 AMeV).  
[19] P. Napolitani and M. Colonna, *Phys. Lett. B* **726**, 382 (2013); P. Napolitani and M. Colonna, *Phys. Rev. C* **92**, 034607 (2015).  
[20] T. Gaitanos, A. B. Larionov, H. Lenske *et al.*, *Phys. Rev. C* **81**, 054316 (2010); A. B. Larionov, T. Gaitanos and U. Mosel, *Phys. Rev. C* **85**, 024614 (2012); O. Buss, T. Gaitanos, K. Gallmeister *et al.*, *Phys. Rep.* **512**, 1 (2012); See also <https://gibuu.hepforge.org>  
[21] F. S. Zhang and E. Suraud, *Phys. Rev. C* **51**, 3201 (1995); W. J. Xie, J. Su, L. Zhu *et al.*, *Phys. Rev. C* **88**, 061601(R) (2013); W. J. Xie, J. Su, L. Zhu *et al.*, *Phys. Lett. B* **718**, 1510 (2013).  
[22] B. A. Li, C. M. Ko, and Z. Z. Ren, *Phys. Rev. Lett.* **78**, 1644 (1997); B. A. Li, C. M. Ko, and W. Bauer, *Int. J. Mod. Phys. E* **7**, 147 (1998); L. W. Chen, C. M. Ko, B. A. Li *et al.*, *Eur. Phys. J. A* **50**, 29 (2014).  
[23] P. Danielewicz and G. F. Bertsch, *Nucl. Phys. A* **533**, 712 (1991); P. Danielewicz, *Nucl. Phys. A* **673**, 375 (2000).  
[24] C. Fuchs and H. H. Wolter, *Nucl. Phys. A* **589**, 732 (1995); T. Gaitanos, M. Di Toro, S. Typel *et al.*, *Nucl. Phys. A* **732**, 24 (2004); G. Ferini, T. Gaitanos, M. Colonna *et al.*, *Phys. Rev. Lett.* **97**, 202301 (2006).  
[25] C. M. Ko and G. Q. Li, *Phys. Rev. C* **37**, 2270 (1988); *J. Phys. G* **22**, 1673 (1996); T. Song and C. M. Ko, *Phys. Rev. C* **91**, 014901 (2015).  
[26] M. Colonna, M. Di Toro, A. Guarnera *et al.*, *Nucl. Phys. A* **642**, 449 (1998); A. Guarnera, M. Colonna, and Ph. Chomaz, *Phys. Lett. B* **373**, 267 (1996); M. Colonna, *Phys. Rev. Lett.* **110**, 042701 (2013).  
[27] A. Ono, H. Horiuchi, T. Maruyama *et al.*, *Prog. Theor. Phys.* **87**, 1185 (1992); *Phys. Rev. C* **47**, 2652 (1993).  
[28] J. Su, F. S. Zhang, and B. A. Bian, *Phys. Rev. C* **83**, 014608 (2011); J. Su and F. S. Zhang, *Phys. Rev. C* **87**, 017602 (2013); J. Su, K. Cherevko, W. J. Xie *et al.*, *Phys. Rev. C* **89**, 014619 (2014).

- [29] C. Hartnack, Z. X. Li, L. Neise *et al.*, Nucl. Phys. A **495**, 303 (1989).
- [30] J. Aichelin, Phys. Rep. **202**, 233 (1991).
- [31] M. Papa, T. Maruyama, and A. Bonasera, Phys. Rev. C **64**, 024612 (2001); M. Papa, G. Giuliani, and A. Bonasera, J. Comp. Phys. **208**, 403 (2006); M. Papa, Phys. Rev. C **87**, 014001 (2013).
- [32] Y. X. Zhang and Z. X. Li, Phys. Rev. C **74**, 014602 (2006); Y. X. Zhang, Z. X. Li, and P. Danielewicz, Phys. Rev. C **75**, 034615 (2007); Y. X. Zhang, P. Danielewicz, M. Famiano *et al.*, Phys. Lett. B **664**, 145 (2008).
- [33] Z. Q. Feng, Phys. Rev. C **84**, 024610 (2011); Z. Q. Feng, Phys. Rev. C **85**, 014604 (2012).
- [34] X. G. Cao, G. Q. Zhang, X. Z. Cai *et al.*, Phys. Rev. C **81**, 061603 (2010); G. Q. Zhang, Y. G. Ma, X. Z. Cai *et al.*, Phys. Rev. C **84**, 034612 (2011); W. B. He, Y. G. Ma, X. G. Cao *et al.*, Phys. Rev. Lett. **113**, 032506 (2014).
- [35] D. T. Khoa, N. Ohtsuka, M. A. Matin *et al.*, Nucl. Phys. A **548**, 102 (1992); V. Uma Maheswari, C. Fuchs, A. Faessler *et al.*, Nucl. Phys. A **628**, 669 (1998); K. Shekhter, C. Fuchs, A. Faessler *et al.*, Phys. Rev. C **68**, 014904 (2003); M. D. Cozma, Y. Leifels, W. Trautmann *et al.*, Phys. Rev. C **88**, 044912 (2013).
- [36] Q. Li, Z. Li, S. Soff *et al.*, Phys. Rev. C **72**, 034613 (2005); Q. Li, C. Shen, C. Guo *et al.*, Phys. Rev. C **83**, 044617 (2011).
- [37] S. A. Bass, M. Belkacem, M. Bleicher *et al.*, Prog. Part. Nucl. Phys. **41**, 255 (1998).
- [38] G. F. Bertsch and S. Das Gupta, Phys. Rep. **160**, 189 (1988).
- [39] R. J. Lenk and V. R. Padharipande, Phys. Rev. C **39**, 2242 (1989).
- [40] P. Danielewicz and G. F. Bertsch, Nucl. Phys. A **533**, 712 (1991).
- [41] M. Papa, G. Giuliani, and A. Bonasera, J. Comp. Phys. **208**, 403 (2005).
- [42] J. Aichelin and H. Stoecker, Phys. Lett. B **176**, 14 (1986).
- [43] W. Botermans and R. Malfliet, Phys. Rep. **198**, 115 (1990).
- [44] P. Danielewicz, Ann. Phys. **152**, 239 (1984).
- [45] G. J. Mao, Z. X. Li, Y. Z. Zhuo *et al.*, Phys. Rev. C **49**, 3137 (1994).
- [46] C. Y. Wong, Phys. Rev. C **25**, 1460 (1982).
- [47] Y. Abe, S. Ayik, P. G. Reinhard *et al.*, Phys. Rep. **275**, 49 (1996).
- [48] H. Feldmeier and J. Schnack, Rev. Mod. Phys. **71**, 655 (2000).
- [49] A. Ono, S. Hudan, A. Chbihi *et al.*, Phys. Rev. C **66**, 014603 (2002).
- [50] M. Colonna, G. F. Burgio, Ph. Chomaz *et al.*, Phys. Rev. C **47**, 1395 (1993).
- [51] Ph. Chomaz, M. Colonna, A. Guarnera *et al.*, Phys. Rev. Lett. **73**, 3512 (1994).
- [52] W. Bauer, G. F. Bertsch, and S. Das Gupta, Phys. Rev. Lett. **58**, 863 (1987).
- [53] J. Rizzo, M. Colonna, and A. Ono, Phys. Rev. C **76**, 024611 (2007).
- [54] B. Liu, V. Greco, V. Baran *et al.*, Phys. Rev. C **65**, 045201 (2002).
- [55] N. Wang, Z. X. Li, and X. Z. Wu, Phys. Rev. C **65**, 064608 (2002).
- [56] D. Vautherin and D. M. Brink, Phys. Rev. C **5**, 626 (1972).
- [57] M. B. Tsang, W. A. Friedman, C. K. Gelbke *et al.*, Phys. Rev. Lett. **86**, 5023 (2001).
- [58] Z. Chajecki *et al.*, arXiv: 1402.5216 [nucl-ex].
- [59] P. Marini, A. Bonasera, A. McIntosh *et al.*, Phys. Rev. C **85**, 034617 (2012).
- [60] S. Wuenschel, R. Dierhoffer, G. A. Souliotis *et al.*, Phys. Rev. C **79**, 061602(R) (2009).
- [61] R. Wada, K. Hagel, L. Qin *et al.*, Phys. Rev. C **85**, 064618 (2013).
- [62] L. Qin, K. Hagel, R. Wada *et al.*, Phys. Rev. Lett. **108**, 172701 (2012).
- [63] M. B. Tsang, T. X. Liu, L. Shi *et al.*, Phys. Rev. Lett. **92**, 062701 (2004).
- [64] J. Rizzo, M. Colonna, V. Baran *et al.*, Nucl. Phys. A **806**, 79 (2008).
- [65] L. W. Chen, B. A. Li, and C. M. Ko, Phys. Rev. Lett. **94**, 032701 (2005).
- [66] M. A. Famiano, T. Liu, W. G. Lynch *et al.*, Phys. Rev. Lett. **97**, 052701 (2006).
- [67] M. B. Tsang, Y. X. Zhang, P. Danielewicz *et al.*, Phys. Rev. Lett. **102**, 122701 (2009).
- [68] D. D. S. Coupland *et al.*, arXiv: 1406.4546 [nucl-ex].
- [69] H. Y. Kong, Y. Xia, J. Xu *et al.*, Phys. Rev. C **91**, 047601 (2015).